https://doi.org/10.5194/egusphere-2026-6646
Preprint. Discussion started: 30 October 2026
© Author(s) 2026. CC BY 4.0 License.

Introducing a Low-Cost Approach for Environmental Monitoring with the Civil Air Patrol (CAP) Aircraft: An Example Addressing Greenhouse Gas Emissions

Edward J. Strobach[1], Elaine Jaross[2], Xinrong Ren[3], Joel Dreessen[4], Paul Walter[5], James S. Wang[4], Maurice Roots[6,7], Julia Famiglietti[2], Austin Turner[2], Phillip Stratton[1,3], Russell R. Dickerson[1,8], Kenneth J. Davis[9,10], and Daniel P. Lathrop[2,11]

[1]Atmospheric and Oceanic Sciences Department, University of Maryland, College Park, MD 20742, USA
[2]Department of Geology, University of Maryland, College Park, MD 20742, USA
[3]NOAA Air Resources Laboratory, College Park, MD 20740, USA
[4]Maryland Department of the Environment, Baltimore, MD 21230, USA
[5]St. Edward's University, Austin, TX 78704, USA
[6]Atmospheric Physics, University of Maryland Baltimore County, Baltimore, MD 21250, USA
[7]NASA Goddard Space Flight Center, Greenbelt, MD 20771, USA
[8]Department of Chemistry, University of Maryland, College Park, MD 20742, USA
[9]Department of Meteorology and Atmospheric Science, Pennsylvania State University, University Park, PA 16802, USA
[10]Earth and Environmental Systems Institute, Pennsylvania State University, University Park, PA 16802, USA
[11]Department of Physics, University of Maryland, College Park, MD 20742, USA

Correspondence: Edward J. Strobach (estrobac@umd.edu)

Abstract. Research aircraft provide essential information about weather, climate forcing, and air quality (AQ). Instrumenting and deploying these aircraft, however, requires substantial investment. Single engine Cessna aircraft flown by the Civil Air Patrol (CAP) offer practical, economical, and widely available platforms for tropospheric sounding of meteorological variables, greenhouse gases (GHGs), and short-lived pollutants. A recent partnership with CAP has led to frequent surveys across the state of Maryland with a Licor 7810 to measure CO_2, CH_4, and H_2O concentrations for GHG analyses and a basic meteorological measurement suite to investigate transport and calculate emission rates (ERs) using the mass balance approach (MBA). The flexibility of multiple aircraft and pilots facilitates surveys at weekly to bi-weekly timescales.

This paper outlines the steps required for a successful operation with the CAP, including flight planning and procedures, instrument calibration, and post-processing. Flights dedicated to GHG sampling are used to demonstrate what the platform can deliver, while the approach itself is general and extends to other areas of environmental monitoring. Examples of CAP flights presented here highlight the strategic targeting of GHG emissions from sources selected through close coordination with the Maryland Department of the Environment (MDE), including frequent visits to landfills, natural gas facilities, and other sources to quantify short-term variability of ERs. Also highlighted are synergistic measurements characterizing GHG plumes from ground to flight level from CAP aircraft and NOAA's Air Resources Car (ARC) during a planned release at the Accident natural gas compressor station (NGCS). The

https://doi.org/10.5194/egusphere-2026-6646
Preprint. Discussion started: 30 October 2026
© Author(s) 2026. CC BY 4.0 License.

documentation of frequent flights from this work and the availability of CAP aircraft in all 50 states demonstrates a scalable solution for frequent spatiotemporal GHG monitoring that addresses anthropogenic impacts, complements regional measurement efforts, and serves as a viable option for validating satellite retrievals.

1 Introduction

Observations of the atmosphere throughout the planetary boundary layer (PBL) and lower free troposphere (LFT) are essential for understanding meteorology and atmospheric chemistry. Control of air quality (AQ) and greenhouse gases (GHGs) are important to protect health and reduce anthropogenic impacts on Earth's climate. Increased awareness of contributions to poor AQ and GHG emissions has promoted strategies to monitor the number of non-attainment days a region experiences (i.e., maximum daily 8-hour average ozone (O_3) > 70 ppb according to the National Ambient Air Quality Standards (NAAQS)) and whether goals are being met in reducing GHG emissions (e.g., Daley et al., 2026; Schafer et al., 2025). Investment towards improved instrument technology and measurement strategies from ground-, aircraft-, and satellite-based platforms has expanded our understanding of harmful criteria pollutants, the chemical pathways that lead to O_3 formation, the role of meteorology in transporting pollution, and the identification of sources responsible for increased emissions of key GHGs (e.g., Acker et al., 2025; Dickerson et al., 2024; Jacob et al., 2022; Caicedo et al., 2021; Duren et al., 2019; Cusworth et al., 2019; Tao et al., 2015; Bush et al., 2015; Loughner et al., 2014; Peischl et al., 2013; Taubman et al., 2006). Despite advancements, a major hurdle in environmental monitoring is developing low-cost solutions that maximize spatial and temporal coverage while at the same time serving as supporting datasets for other measurement efforts. Limitations in spatial and temporal coverage for different measurement platforms, as graphically summarized in Figure 3 of Zhang et al. (2023a), stems from constraints related to affordability, schedule flexibility, and scalability. We expound on these limitations in the next several paragraphs below and argue for a solution that utilizes the Civil Air Patrol (CAP) as a conduit to conduct frequent aerial surveys of AQ and GHGs at a low cost.

Long-term AQ networks such as AirNow and the Aerosol Robotic Network (AERONET) have been around since the 1990s and were developed to enhance the spatiotemporal data record of AQ across a myriad of sites spanning the Contiguous United States (CONUS) and beyond (Dye et al., 2004; Holben et al., 1998). These publicly available measurements are often used to determine regions of poor AQ and evaluate chemical transport models (CTMs) (e.g., Pichugina et al., 2026; Strobach et al., 2024; Campbell et al., 2022; Yahya et al., 2014; Roy et al., 2007). However, measurements from these networks are limited to the surface (AirNow) or only provide column content (AERONET), thus leading to challenges when interpreting the cause of poor AQ, especially in situations where elevated O_3 or $PM_{2.5}$ is transported into a region from afar. Profiling capability from the Tropospheric Ozone Lidar Network (TOLNet) and ozonesondes have provided vertical information in situations where non-local transport results in non-attainment of O_3, such as in the case of stratospheric intrusions (Langford et al., 2022), bay breeze interactions (Kotsakis et al., 2022; Caicedo et al., 2021; Stauffer et al., 2015), and wildfire smoke (Dreessen et al.,

https://doi.org/10.5194/egusphere-2026-6646
Preprint. Discussion started: 30 October 2026
© Author(s) 2026. CC BY 4.0 License.

2016). Tower measurements of GHGs coupled with fast response wind sensors provide information about surface fluxes across an area that depends on the height of the measurement and the meteorological conditions, such as wind shear and atmospheric stability (Zhu et al., 2023; Kljun et al., 2015). Dense networks of towers across urban areas and sources responsible for emitting GHGs (e.g., landfills) have been used to evaluate the spatiotemporal variability of emissions and bottom-up inventories (e.g., Turnbull et al., 2018; Xu et al., 2014), to conduct atmospheric inversions to examine whole city emissions (e.g., Lauvaux et al., 2016), and to understand emissions from sites that vary significantly under meteorological conditions and site operations (Kang et al., 2024; Xu et al., 2014). However, these measurements are either limited to a single point in horizontal space, require an immense amount of investment to fill in spatial gaps and information, are deployed only during field campaigns, or, in the case of eddy covariance GHG flux measurements, are limited in footprint.

Surface and profiling networks are sometimes augmented by in situ and remote sensing measurements from ground-based mobile surveys and aircraft, especially during field campaigns (e.g., Sullivan et al., 2019; Davis et al., 2017; Ryerson et al., 2013). Ground-based mobile measurements have demonstrated the ability to characterize AQ and GHG concentrations at a local neighborhood scale (Dickerson et al., 2024; Bush et al., 2015; Tao et al., 2015). The resolution afforded by ground-based mobile surveys has been instrumental in determining the spatial distribution and variability of hotspots (Bush et al., 2015; Tao et al., 2015), offering comparisons to bottom-up inventories and nearby stationary measurements (Fung et al., 2023; Bush et al., 2015), and assisting in flight operations (Daley et al., 2026). While ground-based mobile measurements enhance spatial information and can pinpoint local causes of AQ and GHG emissions, they are limited to on-road applications where mobility is often hampered by traffic congestion. Slow moving ground-based mobile systems limited to roadways can result in a monumental task when surveying entire cities where revisit times to hotspots vary significantly depending on city layout and driving strategies. Measurements conducted aboard aircraft, by contrast, have more spatial freedom as they are not confined to roads or the ground. Numerous studies over the years have demonstrated aircraft as essential in filling in spatial gaps, estimating emissions of GHGs across large regions and from local sources (Schafer et al., 2025; Daley et al., 2026; Ahn et al., 2020; Ren et al., 2018), evaluating CTMs (Goldberg et al., 2016; Loughner et al., 2014; He et al., 2014), and profiling the structure of plumes along a Lagrangian path (Taubman et al., 2006). However, the downside to aircraft measurements is the long gaps between intensive operation periods (IOPs) limited by affordability and availability as well as practical flight restrictions that limit sampling location and altitude.

The deployment of satellites focused on AQ and GHGs compensate for gaps in the temporal record with frequent revisit times as achieved by hourly retrievals from a geostationary orbit (Zhao et al., 2025; Acker et al., 2025) or across daily to monthly timescales from a sun-synchronous orbit (Ohyama et al., 2024; Guanter et al., 2021; Tang et al., 2020; Hu et al., 2018). Prior to the 2023 launch of the Tropospheric Emissions: Monitoring of Pollution (TEMPO) instrument, AQ-focused satellites have been relatively coarse in both space and time. The 2 km x 4.75 km resolution and hourly retrievals from TEMPO partially resolves the diurnal cycle of O_3, nitrogen dioxide (NO_2), and formaldehyde (HCHO) across urban areas in the CONUS. Recent studies have found good agreement with ground-

https://doi.org/10.5194/egusphere-2026-6646
Preprint. Discussion started: 30 October 2026
© Author(s) 2026. CC BY 4.0 License.

based measurements of O_3 if solar zenith angle and latitude corrections are applied (Zhao et al., 2025) and with ground-based measurements of NO_2 at appreciable distances from roadways (Acker et al., 2025). The spatiotemporal scale of current AQ satellites is still too coarse to resolve sharp AQ gradients across interacting air masses (e.g., synoptic-scale winds and bay breeze interactions) and fine details of the vertical structure (Loughner et al., 2014). Satellites focused on GHGs have increased in number and are designed to target entire areas or major point sources. While whole city emissions can be addressed with area flux mappers, point source satellites (e.g., GHGSat) resolve GHG plumes at 10s of meters. Several recent studies have documented the utility of point source imagers by quantifying emission rates (ERs) from landfills and oil and gas operations around the globe (e.g., Cusworth et al., 2024; Thorpe et al., 2023; Jacob et al., 2022; Duren et al., 2019). The high spectral and spatial resolution of Carbon Mapper and GHGSat has enabled the detection of GHG sources against a heterogeneous background with emission rates as low as 100 kg hr^{-1} (McLinden et al., 2024). However, these satellites operate on a schedule, are in high demand, are constrained by their orbits, and maintain an accessibility cost depending on platform.

To alleviate the spatiotemporal constraints outlined above, we present a low-cost approach that leverages the CAP, a civilian auxiliary for the United States Air Forces (USAF), to conduct frequent aerial surveys of AQ and GHGs in the state of Maryland through a partnership with the University of Maryland, College Park (UMCP), NOAA Air Resources Laboratory (ARL), and the Maryland Department of the Environment (MDE) as part of an effort to develop and enforce Maryland's climate and AQ plans through regulations and updated emissions inventories. While in its infancy, the advantage of hosting AQ and GHG instruments onboard CAP aircraft is owed to a reduction in cost by orders of magnitude ($\approx$ \$100/hour as opposed to thousands per hour for typical research aircraft) and increased availability of aircraft and dedicated CAP pilots. Weekly AQ surveys and revisits of sources emitting GHGs are theoretically possible and would reduce temporal limitations of aircraft from characterizing a specific day or small number of days (as outlined in Figure 3 of Zhang et al. (2023a)) to determining weekly or monthly trends. Moreover, clearance has been given to fly AQ and GHG instruments with CAP in the state of Colorado, thus potentially highlighting scalability to an area the size of the CONUS. In addition, measurements made from CAP aircraft have proven to be an excellent ancillary dataset to other efforts in the region, particularly with respect to field deployments and ground-air coordination activities as demonstrated in this paper. CAP-based flights will not only fill in spatiotemporal gaps and enhance spatial information regarding AQ and GHGs, but could also serve as an additional platform for evaluating CTMs and satellites.

The scope of this paper is deliberately broad in its framing and narrow in its demonstration. The operational approach described here—flight planning, instrument integration, calibration, and post-processing—is not specific to any one measurement, and the same aircraft and procedures apply equally to other areas of environmental monitoring. GHG surveys are featured in this paper as a demonstration to highlight each step in operational planning, from source selection with MDE through to the reporting of ERs. A companion paper takes the same platform in a different direction and examines an AQ episode using an O_3 monitor together with regional profilers, surface networks, and TEMPO (Strobach et al., 2026).

https://doi.org/10.5194/egusphere-2026-6646
Preprint. Discussion started: 30 October 2026
© Author(s) 2026. CC BY 4.0 License.

The remainder of the paper will focus on details regarding the CAP aircraft and instruments onboard (Section 2); supporting regional datasets that include those generated by the Department of Energy (DOE) Atmospheric Radiation Measurement (ARM) Coastal-Urban-Rural Atmospheric Gradient Experiment (CoURAGE) and NOAA's Air Resources Car (ARC) in Section 3; the calibration procedures conducted on the LI-7810 gas analyzer in addition to emission estimation techniques employed using CAP aircraft measurements (Section 4); and results highlighting frequent visits to GHG sources to monitor the structure of plumes, the evolution of ERs using different sampling approaches, and coordinated measurements with ground-based monitoring (Section 5). Section 6 is the conclusions and future direction.

2 Plan Design and Implementation

The recent partnership between the CAP, UMCP, and MDE has fostered frequent low-cost flights across Maryland to identify sources of GHG emissions and to characterize AQ episodes that impact human health, particularly for sensitive groups (e.g., newborns, elderly, immunocompromised, etc.). Availability of multiple aircraft and pilots, a portable and easy-to-operate instrument suite, and the option to fly from different regional airports has supported flexible flight planning.

2.1 CAP Aircraft

Figure 1a shows one of two types of CAP aircraft: the single engine Cessna 172 (C172). The C172 and the larger C182 are four seater aircraft with no walkthrough cabin. The C182 has slightly greater power and a larger payload capacity. Each flight requires a pilot and a support scientist to set-up and operate instruments. All flights since 10 February 2025 have accommodated the Licor (LI) 7810 gas analyzer and a Bad Elf GPS. The duration of flights thus far has ranged between 2 to 4 hours spanning the late morning to early afternoon when the PBL is well-mixed. Flights are limited to fair weather and low wind speed conditions in accordance to visual flight rules (VFRs). Several regional airports and the availability of multiple planes and pilots allows a flexible bi-weekly schedule where the only cost incurred is payment for fuel (≈$100/hour).

2.2 Instruments

In this section, we describe the GHG analyzer and the navigational and meteorological instrumentation onboard CAP aircraft. A dual-beam O_3 monitor was added to the payload beginning on 2 July 2025 for AQ surveys; that instrument, and the AQ case study it supports, are described in the companion paper (Strobach et al., 2026). Instruments operating independent of CAP aircraft are discussed in the Field Deployments and Coordinated Measurements section since that data adds value and spatial context to the measurements conducted from CAP aircraft, and because we want to motivate how the CAP can be leveraged to support other field measurements and operations.

https://doi.org/10.5194/egusphere-2026-6646
Preprint. Discussion started: 30 October 2026
© Author(s) 2026. CC BY 4.0 License.

Figure 1. a) Example of a C172 Cessna used by the Civil Air Patrol (CAP) with b) an inset of the inlet tube from the LI-7810 directed out the window, and c) the LI-7810 secured in the backseat of the C172.

2.2.1 LI-7810

The LI-7810 is a trace gas analyzer for carbon dioxide (CO_2), methane (CH_4), and water vapor (H_2O) that uses the Optical Feedback–Cavity Enhanced Absorption Spectrometer (OF–CEAS) technique to determine concentrations at a 1-second resolution. Figure 1c shows the LI-7810, with an inlet tube attached on the side directed out the window (Figure 1b). In the front is a real-time display above the case handle that reports concentrations and battery status. The instrument is capable of measuring concentrations of CO_2 and CH_4 with a precision of 3.5 ppm at 400 ppm and 0.6 ppb at 2 ppm, respectively.

The LI-7810 can operate up to eight hours on battery power. Replacement of the battery supply can be done during operation without impacting measurements. It takes about 30 minutes for the instrument to warm-up as indicated by the status light sequence on the display. The instrument is monitored in flight from a tablet or smartphone via Wi-Fi. Connecting to the instrument from a computer allows realtime measurements to be displayed, settings to be accessed and changed, and inspection of data features of interest. A separate Python-based code is run after each measurement period to export data encompassing the time range of interest onto a local machine prior to analysis.

2.2.2 CAP Navigational Instrumentation and the Garmin G1000

All CAP aircraft use the Garmin G1000 telemetry log files for integrating and displaying regional weather radar as well as navigational and aircraft data. Files are downloaded from an SD card after each flight, with data including geographical position and altitude, aircraft orientation and acceleration, and meteorological variables, such as flight-

https://doi.org/10.5194/egusphere-2026-6646
Preprint. Discussion started: 30 October 2026
© Author(s) 2026. CC BY 4.0 License.

level winds and temperature. A Bad Elf GPS is included alongside the G1000 to provide an independent record of position and altitude. Both the Bad Elf GPS and the Garmin G1000 flight data are reported at a 1-second resolution and are merged with the LI-7810 record during post-processing once the instrument clock correction described in Section 4.1 has been applied. Flight-level winds from the G1000 are central to this work: together with GHG concentrations they are used to examine the temporal variability of ERs from targets of interest through the mass balance approach (MBA) described in Section 4.3 and to address the spread of the winds sampled along a flight that contributes to ER uncertainties.

2.3 Site Identification and Regional Mapping

Figure 2 shows 26 CAP flights (5 AQ–blue; 21 GHG–light gray) conducted between February 2025 and July 2026 overlaid with sources of GHG emissions and instrumented sites with enhanced measurement capability. Most of the flights focused on targeting specific CH_4 sources in coordination with MDE such as landfills (cyan triangles), natural gas compressor stations (NGCS; yellow circles), and a liquified natural gas (LNG) facility (purple triangle rotated left).

The Atmospheric Radiation Measurement (ARM) Mobile Facilities (AMFs) in Figure 2 were deployed during this time to support the Coastal-Urban-Rural Atmospheric Gradient Experiment (CoURAGE). We leveraged the Doppler lidars (DLs) at the core and supporting AMFs to characterize the PBL and regional winds. Further details on the DL systems are left for Section 3.

2.4 Flight Planning

Flight plans developed so far fall under two categories: 1) GHG source targeting and 2) AQ surveys. This paper is concerned with GHG source targeting while a demonstration of an AQ flight in coordination with other instrumented platforms is described in a companion paper (Strobach et al., 2026). For GHG sampling, we select from a pre-determined list of GHG sources identified by MDE and UMCP. From there, a flight plan is developed that typically includes tight spirals around GHG sources at different heights. If the flight plan permits, then a second sampling of a particular source at a later time is conducted to examine short-term variability of emissions.

The spirals conducted around GHG targets of interest during most flights are well suited for compact sources but become difficult to execute around spatially extensive targets such as large landfills. Circling close enough to a large source can result in a turning radius that is sharp enough to contaminate flight-level winds (Section 4.3 and Figure S1), while a spiral flown at a radius large enough to avoid that contamination may no longer intersect the plume centerline at every level. These practical challenges motivated an alternative approach in which the aircraft flies a lawnmower pattern in the horizontal and a sawtooth pattern in the vertical, filling a downwind volume rather than encircling the source. The mass balance formulation this pattern supports is described in Section 4.3, and an example of this modified approach for the Route 40 West landfill is presented in Section 5.3.

https://doi.org/10.5194/egusphere-2026-6646
Preprint. Discussion started: 30 October 2026
© Author(s) 2026. CC BY 4.0 License.

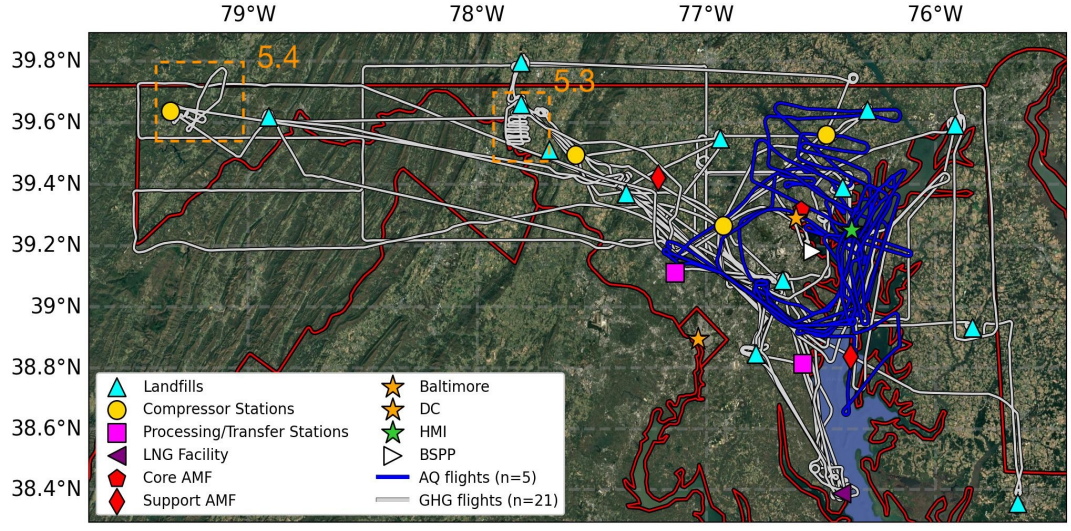

Figure 2. A composite of 26 CAP flights conducted spanning 10 February 2025 – 15 July 2026. Overlaid on the map are GHG sources separated by type (landfills–cyan triangles; natural gas compressor stations–yellow circles; LNG facility–purple triangle rotated to the right; and processing/transfer stations for solid waste and recycling–magenta squares). Also shown are the atmospheric radiation measurement (ARM) mobile facility (AMF) core (red pentagon–Baltimore) and ancillary (red diamonds–Kent Island and Mt. Airy) sites from the Coastal-Urban-Rural Atmospheric Gradient Experiment (CoURAGE), the Brandon Shores Power Plant (BSPP–white triangle rotated to the right), the cities of Baltimore and Washington, DC (orange stars), Hart Miller Island (HMI–green star), and AQ (blue) and GHG (light gray) flights. Orange dashed boxes outlining portions of the flight highlight comprehensive sampling of a GHG plume and coordinated activities discussed in sections 5.3 and 5.4, respectively. State boundaries are shown by the red lines. Google Earth imagery © 2025 Google.

An assessment of weather conditions and airspace restrictions is imperative prior to the development of a flight plan. If weather conforms to CAP rules, then SkyVector is used to create a flight plan that is submitted for review prior to deployment. Restrictions are in place across certain areas (e.g., the nation's capital and Aberdeen Proving Ground) that limit the range of heights we can fly, or, depending on location, results in a no fly zone. Most of the sources sampled are outside of the no fly zone. Special requests must be made in advance to accommodate flights in restricted air space. When possible, a portion of the flight is dedicated to determining the height of the PBL to identify the heights at which the plume was sampled relative to the PBL.

3 Field Deployments and Coordinated Measurements

Most of the flights conducted so far temporally overlapped with the CoURAGE (Davis et al., 2024). Outside of CoURAGE, coordinated measurements were also conducted with NOAA's Air Resources Car (ARC), a mobile

https://doi.org/10.5194/egusphere-2026-6646
Preprint. Discussion started: 30 October 2026
© Author(s) 2026. CC BY 4.0 License.

ground-based laboratory that was operated jointly with the CAP aircraft during a planned natural gas release event. Below we describe the observations used in conjunction with CAP flight measurements.

3.1 Coastal-Urban-Rural Atmospheric Gradient Experiment (CoURAGE)

CoURAGE was funded by the U.S. Department of Energy (DOE) Atmospheric Systems Research (ASR) program to deploy Atmospheric Radiation Measurement (ARM) Mobile Facilities (AMF1; Miller et al., 2016) to Mt. Airy (rural site), Baltimore (urban), and Kent Island (Chesapeake Bay) to address differences across the rural-urban-bay interfaces related to regional dynamics, the development of convection across a heterogeneous surface, and pollution transport. CoURAGE occurred from 1 December 2024 to 30 November 2025 with intensive operating periods (IOPs) featuring enhanced observations from 11-25 February 2025 and 14-28 July 2025. Data from DLs located at these sites are used to determine the horizontal and vertical wind structure as well as the time evolution of winds when CAP aircraft were in flight. The locations of the AMFs are shown by red plot symbols in Figure 2, with the core site (Baltimore) represented by a pentagon and the supporting sites (Mt. Airy and Kent Island) represented by diamonds.

3.1.1 Doppler Lidars (DLs)

The DLs deployed to AMFs sites for the CoURAGE effort were designed and developed by Halo Photonics to characterize the PBL wind and turbulence structure. The DL at the CoURAGE sites operated a conical scan to derive horizontal winds and conducted vertical stares to characterize the vertical velocity and turbulence structure. For this work, we only evaluate the horizontal winds to understand flow steadiness and uniformity during a CAP flight as well as the vertical wind shear structure and mesoscale wind patterns.

The conical scans conducted by AMF DLs were programmed with a laser subtended 30° from nadir and rotated azimuthally along six positions (i.e., 60° separation between azimuthal angles). A sinusoidal fitting procedure using velocity azimuth display (VAD) at each range gate was conducted to convert the radial winds into a horizontal wind product (Browning and Wexler, 1968). The condition of homogeneity across the scanning volume (i.e., winds along opposing beam positions must be similar in magnitude) was employed by only accepting sinusoidal fits to the line-of-sight winds with a correlation coefficient of 0.8 or greater. The vertical separation between range gates along the beam was 30 m, and thus provided highly resolved details of the vertical structure of horizontal winds. The time to complete a single scan to derive horizontal winds was 10 minutes, which was essential in order to gather enough signal to determine a velocity distribution. Profiles from DLs during flights are used to assess wind uncertainty are available in the Supplementary Materials.

https://doi.org/10.5194/egusphere-2026-6646
Preprint. Discussion started: 30 October 2026
© Author(s) 2026. CC BY 4.0 License.

3.2 NOAA's Air Resources Car (ARC)

NOAA's ARC is a mobile atmospheric measurement platform designed to characterize the spatial distribution, source signatures, and emission enhancements of GHGs and air pollutants at a high spatiotemporal resolution across urban, industrial, agricultural, and rural environments. Its integrated instrumentation includes (1) a Picarro G2401 cavity ring-down spectrometer (CRDS) for continuous measurements of CO_2, CH_4, CO, H_2O; (2) a Picarro G2201-i CRDS analyzer for measurements of ^{13}C isotopic composition of CH_4 and CO; (3) a 2B Technologies ozone analyzer; (4) an Aeris Ultra MIRA spectrometer for C_2H_6; (5) a Direct Optics G60 CRDS analyzer for nitrogen oxides (NO, NO_2, and NO_x), (6) an AE43 Aethalometer for black carbon at seven wavelengths; and (7) a Particle Plus sensor for $PM_{2.5}$ and PM_{10}. The platform is also equipped with a differential GPS and high-frequency meteorological sensors, including wind speed and direction, temperature, pressure, and humidity, enabling atmospheric concentrations to be mapped relative to local transport conditions and emission sources. Together, these measurements allow NOAA's ARC to identify and characterize localized plumes from fossil-fuel infrastructure, landfills, wastewater facilities, agricultural operations, transportation, and other urban sources. Measurements of CH_4 together with C_2H_6 and stable carbon isotopes provide valuable source-attribution capability, helping distinguish thermogenic fossil-fuel emissions from biogenic methane sources. NOAA's ARC is particularly effective when operated in coordination with an aircraft, providing complementary observations near the surface while the aircraft characterizes the vertical distribution and regional transport of pollutants.

4 Methodology

Strategic flights focused on intercepting GHG emissions from selected sources have resulted in the isolation and quantification of CH_4 and CO_2 plumes. Optimal flight paths near targets of interest at different heights have provided the data needed to estimate ERs, which has been valuable when reporting separately to MDE and facility operators about how much mass is leaving the source. This collaboration supports Maryland's climate initiative in reducing GHG emissions to net-zero by 2045 (i.e., https://www.epa.gov/system/files/documents/2024-03/mde-state-of-maryland-cprg-priority-climate-action-plan.pdf). Here, we describe calibration procedures for the LI-7810, an approach to isolate GHG plumes from the background, the mass balance approach (MBA) for estimating ERs, the Kriging approach for volumetric plume sampling, and flight-level ethane (C_2H_6) derived from ground-based measurements that will be useful for estimating C_2H_6 ERs during coordinated activities.

4.1 Calibration Procedures

Laboratory tests with the LI-7810 have been conducted to understand how measurements change with pressure and drift with time. Although the instrument was designed to conduct reliable measurements in a reduced pressure environment, tests were still conducted at NOAA ARL within a pressure chamber to determine how much CO_2 and

https://doi.org/10.5194/egusphere-2026-6646
Preprint. Discussion started: 30 October 2026
© Author(s) 2026. CC BY 4.0 License.

Table 1. CH_4 and CO_2 calibration tank concentrations and their corresponding tank number.

Tank No.	CO_2 (ppm)	CH_4 (ppb)
# 18	460.58	2529.1
# 19	423.48	1925.4
# 21	495.8	2296.7

CH_4 artificially drifted with a decrease in atmospheric pressure. Other considerations in the data relate to the time it takes for air to flow through the tubing into the instrument and a mismatch between the internal clock of the LI-7810 and universal time. Comparisons between universal time and instrument time are conducted prior to flight take-off where the difference is used to correct the instrument time, while an additional time correction is applied that accounts for the length of the tubing and the flow rate of air into the instrument. Together, these corrections are applied so that measurements from other instruments can be paired with the LI-7810 when analyzing the data and calculating ERs.

4.1.1 Measurement Drift with Time

Measurements of CO_2 and CH_4 from the LI-7810 drift over time with increased use of the instrument. This results in increasingly larger departures between measured concentrations compared to the true concentrations. Ideally, these departures should be evaluated before each flight to examine how much of a difference there is between measured concentrations versus actual concentrations. This is done by comparing calibrated gas tank concentrations in Table 1 with measurements from the LI-7810 when calibration gas is fed into the instrument. The difference between calibration gas concentrations and measured concentrations from the three tanks are used to derive slopes and offsets as corrections applied to measurements after each flight. The slopes and offsets are determined by a line of best fit via

$$[X]_t = m[X]_{meas} + b \tag{1}$$

where $[X]_t$ and $[X]_{meas}$ are time-drift adjusted concentrations and measured concentrations, respectively, of CO_2 or CH_4, and m and b are slopes and offsets derived from comparisons with calibration tanks and applied to measurements as a correction. Three tanks are suitable for calibration since we do not expect variation outside the line of best fit nor do we expect nonlinear behavior. These corrections are essential if we are interested in accurately reporting concentrations and estimating ERs. Figure 3a-b shows an example comparing tank-rated values of CO_2 (Figure 3a) and CH_4 (Figure 3b) versus measured values with slopes and offsets reported in the legend. Calibration values have been determined before many of the flights conducted so far.

https://doi.org/10.5194/egusphere-2026-6646
Preprint. Discussion started: 30 October 2026
© Author(s) 2026. CC BY 4.0 License.

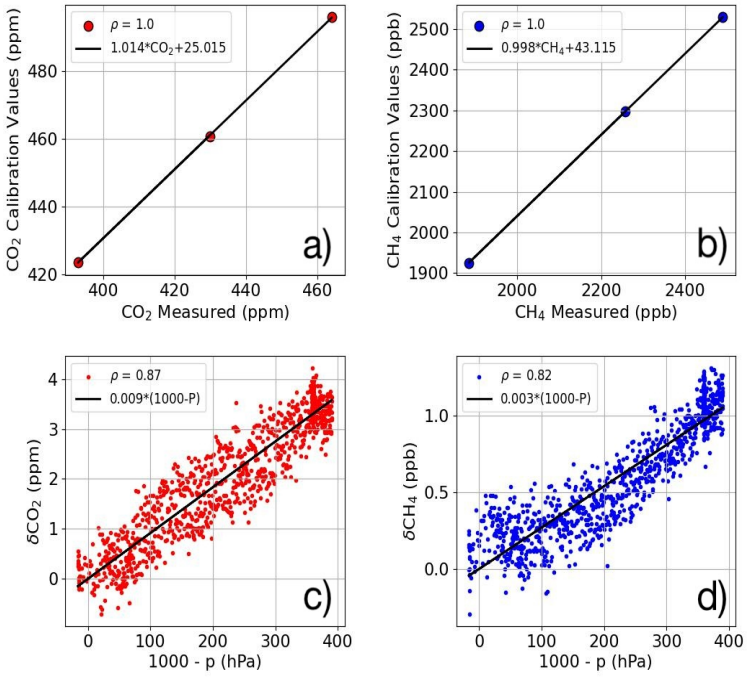

Figure 3. Calibration tests conducted 20 February 2025 against rated tank values in Table 1 for a) CO_2 and b) CH_4. Pressure chamber tests showing how c) CO_2 and d) CH_4 change as a function of $1000 - p$, where p is pressure. Lines of best fit are shown for all four panels along with slopes, offsets, and correlation coefficients reported in the legend. While the time drift should be evaluated before each flight, the pressure dependence of LI-7810 GHG measurements only needed to be evaluated once using NOAA ARL's pressure chamber.

4.1.2 Pressure Dependence of Measured Concentrations

The LI-7810 was placed in a pressure chamber to determine whether concentrations changed when environmental pressure decreased, and if so, by how much. Figure 3c-d shows how CO_2 (red) and CH_4 (blue) increase as pressure deviates from a reference value of 1000 hPa, i.e., $1000 - p$. A 400 hPa departure from 1000 hPa reveals a difference of about 1 ppb and 4 ppm for CH_4 and CO_2, respectively. The lowest pressures measured during flights so far have been about 900 hPa or a little over 800 m from the surface. A maximum departure of 100 hPa from a reference value of 1000 hPa suggests that pressure effects were at most 0.3 ppb and 1 ppm, respectively, for CH_4 and CO_2 based on Figure 3c-d. This indicates that our measurements were minimally affected and that the variation in Figure 3c-d is comparable to the range of values along the best fit for the first 100 hPa of departure from a reference value of 1000 hPa. If needed, a correction accounting for the effect of pressure can be applied during post-processing prior to

https://doi.org/10.5194/egusphere-2026-6646
Preprint. Discussion started: 30 October 2026
© Author(s) 2026. CC BY 4.0 License.

analysis using

$$\delta[X]_p = [X]_p - X_0 = \frac{\Delta X}{\Delta p}(1000 - p) \tag{2}$$

where $[X]_p$ are pressure-adjusted concentrations at a given pressure, p, and $\frac{\Delta X}{\Delta p}$ and X_0 are slopes and offsets derived from fitting how baseline concentrations in a chamber change with pressure. The offset in Equation (2) is brought to the other side where $\delta[\mathrm{X}]_p$ represents $[\mathrm{X}]_p$-X_0. Adding Equations (1) and (2) leads to fully corrected measurements accounting for time and pressure drift, i.e.,

$$[X]_{corr} = [X]_t(p) + \delta[X]_p \tag{3}$$

where $[X]_{corr}$ represents fully corrected concentrations while $[X]_t(p)$ represents the time-corrected portion as a function of pressure.

4.2 Plume and Background Identification

For spirals conducted around GHG sources, plumes were identified by sharp increases in CH_4 well above background concentrations, where background CH_4 is defined as concentrations near the plume within the PBL that are less than or equal to plume edge values. Plume concentrations are determined by inspecting a time series generated in Python. Zoom-in capability available within the plotting window allows plumes to be isolated and the indices associated with plume edges determined and stored. After working through the time series and recording all indices, a user prompt is issued in Python's command line requesting starting and ending indices for segments of data corresponding to plumes. Indices are used to store location, altitude, GHG concentrations, and flight-level meteorology into netcdf files. A netcdf file is created for each instance a plume is intercepted where the files are used later for plume-focused analyses.

Figure 4a shows a flight with sharp increases in CH_4 overlaid against green shading. The green shading represents starting/ending indices reported in Python's command line when identifying CH_4 plumes. A zoom-in of plumes intercepted downwind of the Millersville landfill in Figure 4b shows reasonable isolation. Identifying plumes in this way gives the user control to avoid selecting peaks that might be erroneous when using automated approaches. Furthermore, the subjective approach avoids over-selecting or under-selecting plumes since the user sets the boundaries for plume edges.

Background concentrations were determined by identifying instances near the plume within the PBL where CH_4 was less than or equal to plume edge concentrations ($[CH_4]_{pe}$). Only concentrations within 5 km (10 km in the case of the Brown Station landfill given its size) of GHG plumes were processed. Additional conditioning was applied to remove values smaller than $[CH_4]_{pe} - 2\sigma$ from the initial background sample and to avoid selecting concentrations during subsequent visits since shifts in air mass can influence local background concentrations in a non-negligible manner. An example of background concentrations is shown by a yellow segment in the CH_4 time series in Figure 4. It is clear that only concentrations near the plumes were selected with values consistently lower than $[CH_4]_{pe}$.

https://doi.org/10.5194/egusphere-2026-6646
Preprint. Discussion started: 30 October 2026
© Author(s) 2026. CC BY 4.0 License.

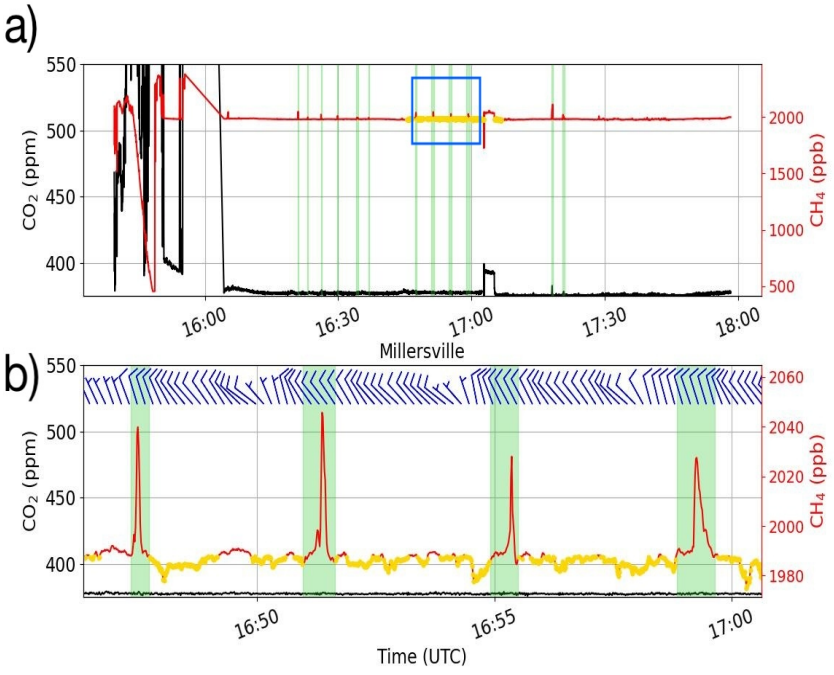

Figure 4. A time series of CO_2 (black) and CH_4 (red) on 3 December 2025 a) for the entire duration flown and b) when the CAP aircraft circled the Millersville landfill. The green shading in both plots indicates the peaks selected subjectively as outlined in Section 4.2. The blue rectangle in a) represents the zoom-in plot in b), which highlights the precision in isolating plumes across sharp peaks out to the diluted edges of the plume. Included in a) are example segments highlighting background CH_4 concentrations in yellow. Flight-level winds are shown in b).

4.3 Estimating Emission Rates (ERs) from the Mass Balance Approach

A common technique to estimate ERs from point sources is to employ the MBA to quantify how much gas is emitted by a particular source per unit time. This requires flying across an area that is transverse to the direction of the plume. Equation (4) represents the area integrated flux of a gas across the width and depth of a plume

$$ER = \int\int (|\boldsymbol{V} \times \hat{r}_{CAP}|)(C - [C])dx\,dz \tag{4}$$

where the term in the first set of parentheses is the magnitude of the cross-product between the vector wind and the direction of the CAP aircraft (i.e., $|\boldsymbol{V} \times \hat{r}_{CAP}|$), the term in the second set of parentheses is the measured concentrations, C, minus the background, $[C]$, and dx and dz are limits of integration across the width and depth of the plume, respectively. MBA has been used extensively in GHG studies over urban environments (Schafer et al., 2025; Ahn et al., 2020; Ren et al., 2018), coal plants (Ahn et al., 2020), agricultural operations (Daley et al., 2026), landfills (Ren et al., 2018; Cambaliza et al., 2017, 2014), and oil and gas operations (Daley et al., 2026; Huang et al., 2024; Conley et al., 2017; Gordon et al., 2015). ERs calculated by MBA compared to satellite retrievals have yielded

https://doi.org/10.5194/egusphere-2026-6646
Preprint. Discussion started: 30 October 2026
© Author(s) 2026. CC BY 4.0 License.

similar estimates despite being reported on different days (Gillespie et al., 2025). The extensive use of MBA lends support to its robustness in quantifying the rate of emissions coming from sources by evaluating GHG fluxes when plumes are intercepted.

For this work, flights transverse to the direction of plume propagation at multiple heights were conducted while simultaneously measuring winds from CAP instruments and GHG concentrations from the LI-7810. To utilize MBA, Equation (4) is re-expressed using summation notation, i.e.,

$$ER = \sum_{k=1}^{N-1} \left[\sum_{i=1}^{M-1} \left(\overline{V \sin(WD - \phi_{CAP}) \Delta C} \, \Delta x \right) \Big|_{i}^{i+1} \right] \Delta z \Big|_{k}^{k+1} \tag{5}$$

where M is the number of measurements across a plume at a particular height, N is the number of vertical levels, WD is the wind direction, ϕ_{CAP} is the orientation of the aircraft, and ΔC is enhancement in concentration above background (i.e., C-[C]). The sine term results from the magnitude of the cross-product in Equation (4), where flights perpendicular to WD maximize the function. The overbar in Equation (5) is an average between consecutive measurements, i and $i+1$, along the plume, while Δx and Δz represent horizontal distances and separation between heights, respectively.

Several factors contribute to uncertainty when estimating ERs (e.g., Daley et al., 2026; Huang et al., 2024; Ahn et al., 2020; Conley et al., 2017; Gordon et al., 2015) that are addressed with different approaches when estimating uncertainty (Gordon et al., 2015). How uncertainty is considered in the MBA depends on the scale of the source region and whether the area encompasses a single source or an aggregation of sources. The main contributions to uncertainty include emissions from sources that drift into and out of the MBA domain (Huang et al., 2024), the representativeness of PBL height (Daley et al., 2026; Ahn et al., 2020), variability of wind measurements (Huang et al., 2024; Ahn et al., 2020), assumptions regarding the vertical profile structure (Daley et al., 2026; Huang et al., 2024; Gordon et al., 2015), the representation of the background concentrations, and the transience of emissions (Huang et al., 2024). The majority of our flights targeted local emissions by conducting tight spirals with radii several kilometers from the source at a time scale spanning several minutes to about an hour. As a result, the uncertainties associated with transient emissions and emissions drifting in and out of the spiral are not of concern. However, assumptions regarding the vertical profile, background concentrations, and the representativeness of winds and PBL height may still be an important consideration. Furthermore, the accuracy of our ER estimates depends on whether the centerline of the plume was approximately intersected at all heights sampled.

4.3.1 Estimating ERs By Flying a Tight Spiral Configuration

In our original approach, we considered profiles from DLs at the DOE ARM CoURAGE sites to address the winds from the surface to flight-level. Occasionally, however, there was strong disagreement between the DLs and the CAP, especially when mesoscale forcing dominated over large-scale forcing that resulted in highly variable winds across space and time. The lack of agreement between the DL and CAP winds on certain days (Table S1) and the contamination of winds when rapidly flying around a source (Fig. S1) resulted in the decision to estimate uncertainty

https://doi.org/10.5194/egusphere-2026-6646
Preprint. Discussion started: 30 October 2026
© Author(s) 2026. CC BY 4.0 License.

by considering winds along flight segments of data ± 30 minutes before and after the interception of plumes for a particular target. This ensured consistency across all targets sampled while considering the spatiotemporal variability of the winds when addressing uncertainties in the MBA.

For background concentrations, we processed data segments using the approach discussed in Section 4.2. We opted to not consider PBL height in our uncertainties since flights featuring spirals were conducted only several kilometers from the source. The close proximity of the aircraft to the source does not support the fetch required for the plume to become well-mixed and reach the height of PBL in many situations, even under a modest horizontal wind. The majority of measurements conducted by the CAP where plumes were intercepted occurred between 220 m and 750 m, which when compared to PBL heights ranging between 1 km and 1.5 km derived from the CoURAGE DLs spanning 10 February 2025 to 28 October 2025, suggests that measurements were conducted exclusively within the mixed layer. The lack of information above and below these heights is an extra source of uncertainty that was not accounted for in our calculations.

Another assumption not considered is uniform CH_4 profiles outside of the height range or extrapolations to the surface. Some studies assume uniform CH_4 concentrations across the vertical or extrapolate to the surface to fill in measurement gaps (e.g., Gordon et al., 2015; Karion et al., 2013). These assumptions and approaches may not be valid when measuring in close proximity to the source since the plume may not have experienced sufficient enough mixing. Therefore, we have no basis for applying this assumption for ER calculations at close distances.

The uncertainties were addressed by randomly selecting from a subset of background concentrations and winds using a Monte Carlo approach when iteratively estimating ERs. We varied the number of selections and found 100 to be a reasonable estimate for statistical convergence when assessing uncertainty. The mean and standard deviation of the separate realizations are quantified and reported in Table 2 and later in Figure 7.

Figure 5a-c shows four loops around the Millersville landfill on 3 December 2025 spanning a height range between 279 m and 530 m. The winds were from the northwest across the layer sampled with the loops maintaining a consistent radius of about 2 km from the landfill. The plumes in Figure 5c are identical to the plumes in Figure 4b but with plume edge values of CH_4 removed and placed on a common axis. The widths and approximate enhancement above background ranged between 1.3-2.5 km and 40-60 ppb, respectively. Randomly selected winds and background concentrations using the Monte Carlo approach described above followed by calculating the inner sum at each height before summing across each vertical layer results in 100×100 ER estimates (100 realizations for winds and background each and their combinations) where an average and standard deviation (uncertainty) is calculated. Most flights conducted to date have featured 2-6 loops around GHG targets across the mixed layer within a 15 minute period. Exceptions include a flight downwind of Eastern Sanitary landfill on 3 March 2025 featuring two straight segments separated by an hour (i.e., Figure 7a), a lawnmower+sawtooth flight across the Route 40 West landfill plume (Section 5.3), and coordinated measurements with NOAA's ARC of GHG emissions from a planned release at the Accident NGCS (Section 5.4). More details from GHG flights are presented in the Greenhouse Gas Surveys section under Results (Section 5).

https://doi.org/10.5194/egusphere-2026-6646
Preprint. Discussion started: 30 October 2026
© Author(s) 2026. CC BY 4.0 License.

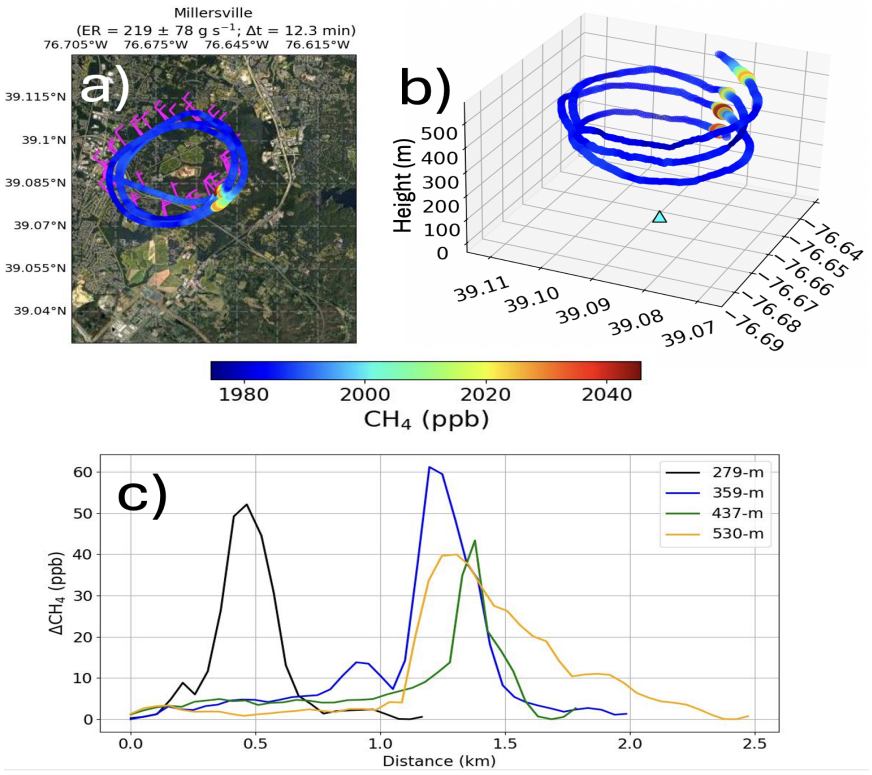

Figure 5. a) Map showing circles conducted around Millersville on 3 December 2025 with the shading representing CH_4 and magenta barbs representing flight-level winds (Google Earth imagery © 2025 Google), b) a 3D rendering of the spiral conducted around Millersville, and c) CH_4 plumes during four passes within a 12 minute period placed on a common axis.

4.3.2 Estimating ERs By Flying a Lawnmower+Sawtooth Configuration

Some challenges capturing GHG plumes emitted by large point sources led to the adoption of lawnmower+sawtooth flights idealized as a cartoon in Figure S2. The portion of the flight that intercepted GHG plumes were identified by isolating downwind segments and filtering out turnaround points (i.e., when aircraft heading rapidly changed). Figure 6a highlights downwind segments that intercepted GHG emissions from the Route 40 West landfill at different downwind distances ranging from 200 m to 14.5 km. The majority of flight segments were nearly constant in height across an altitude range of 200-550m.

A Kriging approach and the inclusion of synthetic observations at the surface using the bottommost leg in Figure 6a was adopted to recast the downwind GHG measurements onto a grid following Krautwurst et al. (2017) as shown in Figure 6b. This was done by applying an exponential semivariogram model, $\gamma(h)$, in Equation (6)

$$\gamma(h) = c_0 + c_1 \cdot \left(1 - e^{-3h/R}\right) \tag{6}$$

https://doi.org/10.5194/egusphere-2026-6646
Preprint. Discussion started: 30 October 2026
© Author(s) 2026. CC BY 4.0 License.

to determine the nugget (c_0), partial sill (c_1), and the range (R) in addition to assessing spatial correlations across the plume at different distances, h, when assigning weights and producing the results in Figure 6b. In this study, vertically averaged Kriged-derived concentrations from Figure 6b were fitted to a Gaussian (Figure S3) to separate background concentrations (Figure 6c) from enhanced concentrations (Figure 6d) using 3σ as the bounds of the plume. Additionally, the winds and temperature followed linear interpolation instead of ordinary Kriging interpolation. The result from Figure 6d with gridded winds and temperature are used as direct input into Equation (5).

The uncertainties in wind speed and direction, Kriging model, background estimation, and surface concentrations were all considered in the analysis. This was accomplished by calculating the standard deviation about the mean to address the variability of wind speed and direction across the plume, multiplying R arbitrarily by 0.25 and 4 while keeping c_0 and c_1 fixed to assess the sensitivity of selecting a range where the fit converges near or far from the source, adjusting plume bounds from 2.5σ to 3.5σ to address uncertainty in background concentrations, and multiplying synthetic observations at the surface by a factor ranging from 0.5 and 1.5.

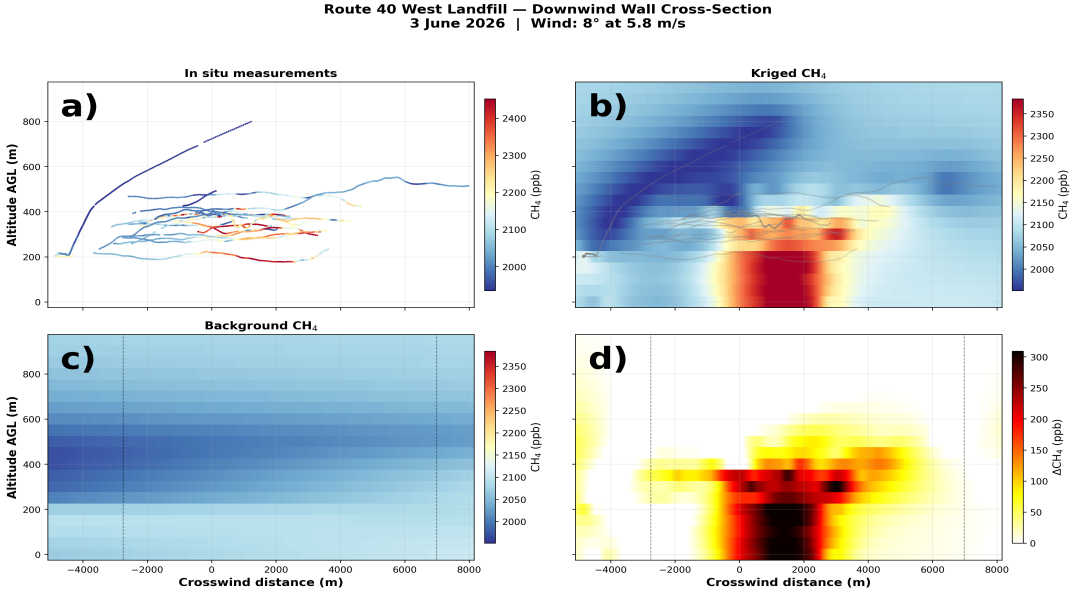

Figure 6. a) In situ CH_4 measurements from the LI-7810 plotted against crosswind distance and altitude AGL along the lawnmower and sawtooth flight pattern. b) Measurements from a) kriged onto a downwind wall with the flight track overlaid in gray. c) The height-dependent background field constructed from the portions of the wall away from the plume. d) The CH_4 enhancement above background, ΔCH_4, that is used in Equation (5). Vertical dashed lines in c) and d) mark the $\pm 3\sigma$ crosswind bounds of the Gaussian fit to the altitude-averaged enhancement profile shown in Figure S3.

https://doi.org/10.5194/egusphere-2026-6646
Preprint. Discussion started: 30 October 2026
© Author(s) 2026. CC BY 4.0 License.

4.4 CH_4 to C_2H_6 Ratios

Coordination between ground-based and aircraft measurements of nonreactive tracers supports the calculation of ratios to infer airborne concentrations of unmeasured species. The payload on NOAA's ARC includes CH_4 and ethane (C_2H_6), while measurements aboard CAP aircraft only include CH_4. Both CH_4 and C_2H_6 are emitted by NGCS, and thus coordinated measurements between ground-based and airborne platforms can be used to infer C_2H_6 at flight level. This is accomplished by calculating the following ratio in Equation (7)

$$[C_2H_6] = \frac{\delta C_2H_6}{\delta CH_4}[CH_4] + \psi_0 \tag{7}$$

where measured $[C_2H_6]$ and $[CH_4]$ from NOAA's ARC is used to derive a slope, $\frac{\delta C_2H_6}{\delta CH_4}$, and offset, ψ_0, that is applied to airborne measurements of CH_4 to derive C_2H_6. The advantage of deriving C_2H_6 at flight-level will allow mass flux estimates in the absence of airborne C_2H_6 when ground and airborne assets coordinate over the same source.

5 Greenhouse Gas Surveys

The majority of CAP flights have focused on identifying GHG sources and measuring CH_4 and CO_2 concentrations. Earlier flights in the winter of 2025 were experimental and demonstrated the coverage achievable with CAP aircraft and the interception of several plumes downwind of different sources in Maryland and across state lines into Pennsylvania and West Virginia.

5.1 Methane ERs from Targeted Sources

More than a dozen flights conducted so far have focused on targeting GHG emission sources, almost all of which have featured tight spirals around a source to intercept plumes at different heights. Figure 7 shows several examples of flight segments around facilities with spirals approximately centered at the facility location. The notable exception is the flight conducted downwind of the Eastern Sanitary landfill, which featured two straight segments spaced an hour apart. In each panel are CH_4 concentrations, flight-level winds, and ERs along with the time it took to sample downwind for the Ellicott City NGCS (b-c, e-f); several landfills that include the Eastern Sanitary landfill (a), Harford Waste Disposal Center (d), Route 40 West (g), and Brown Station (h); and a LNG facility at Cove Point, Maryland (i). The spirals conducted around most of the facilities helped minimize the sampling time to 15 minutes or less to preserve steady state conditions and to avoid transient emissions. The number of loops across heights where the plume was intercepted varied between 2 and 6 for the different sites surveyed, which according to Conley et al. (2017) is far below the minimum number of loops required to minimize uncertainty. While Conley et al. (2017) determined the minimum number of loops required, it is likely that a trade-off exists such that fewer loops around sources at a greater spacing could still lead to similar ER estimates. Noting the lack of information below and above the heights sampled, we acknowledge that this could result in unquantified uncertainties. Primary

https://doi.org/10.5194/egusphere-2026-6646
Preprint. Discussion started: 30 October 2026
© Author(s) 2026. CC BY 4.0 License.

contributors to uncertainty considered are the representation of winds and background concentrations as described in Section 4.3.

It is clear that the plumes in each of the panels can be identified through visual inspection. The approximate width of the plume at each level was estimated using the approach described in Section 4.2, which when examining Figure 7, corresponds to a transition to darker blue shading along the flight segment that is representative of background concentrations at distances away from the plume edge. The winds overlaid on flight segments are uniform across most of the panels shown. Exceptions include the Ellicott City NGCS (Fig. 7f), Route 40 West (Fig. 7g), and Cove Point (Fig. 7i). Increasing the radii of spirals to prevent excessive turning would be ideal so that the winds are not contaminated. For instance, the wind barbs in Figure 4b are nearly uniform and represent an ideal measurement, while the wind barbs in Figure S1 within Supplementary Materials show how winds can vary as the heading varies. The contamination due to excessive turning further motivated the use of winds along straight segments ± 30 minutes before and after plumes were sampled as noted in Section 4.3. Also of note is the misalignment between flight direction and the plume orientation for a couple of cases (e.g., Brown Station (Figure 7h) and Cove Point (Figure 7i)). Better alignment over these sources in the future will be important when determining the true width and concentrations of the plume being intercepted.

Several of the landfills sampled in this study were also sampled in 2015 as reported by Ren et al. (2018): Brown Station, Eastern Sanitary, Harford Waste Disposal Center, Reich's Ford, and Route 40 West. ERs from the Brown Station landfill in Table 2 were 1775±1422 g s^{-1} and 1282±1253 g s^{-1}, which falls within the range of uncertainty for all days estimated by Ren et al. (2018). However, when considering only the average ER, it is clear that our estimates were quite a bit larger by a factor of two or more. The closest comparison between Ren et al. (2018) and our lowest average estimate of 1282 g s^{-1} is 749 g s^{-1} on 24 February 2015. It is important to note that we were much closer to Brown Station than Ren et al. (2018) and we did not intercept the plume perpendicular to its propagation direction (refer to Figure 7h). Similar to Brown Station, the Harford Waste Disposal Center and Reich's Ford agreed within the range of uncertainty reported by Ren et al. (2018) but with average ERs a little lower than what they found. While our estimates for Harford Waste Disposal Center and Reich's Ford were lower, the difference is smaller compared to ERs estimated for Brown Station between Ren et al. (2018) and this study. The Eastern Sanitary landfill in Table 2 and Figure 7a, on the other hand, showed strong agreement with Ren et al. (2018). Only the Route 40 West landfill exhibited differences that exceeded the range of uncertainty calculated, with Route 40 West well above the Ren et al. (2018) study by a large margin (≈2000 g s^{-1} compared to ≈100 g s^{-1}). It should be noted, however, that Route 40 West is one of the largest producers of CH_4 by a landfill in the state of Maryland (https://mde.maryland.gov/programs/air/ClimateChange/Pages/GreenhouseGasInventory.aspx, last access 18 September 2026), so it stands to reason that this source will produce larger ERs than almost all the other sources listed in Table 2. Moreover, the top emitters according to this study—Brown Station and Route 40 West—emitted wider plumes that had much larger enhancements above background compared to the other sources (Table 2), which would naturally lead to larger ERs. However, it should be kept in mind that the lack of measurements

https://doi.org/10.5194/egusphere-2026-6646
Preprint. Discussion started: 30 October 2026
© Author(s) 2026. CC BY 4.0 License.

Table 2. List of GHG targets by source type, the dates targeted, maximum CH_4 concentrations of plumes, and calculation of ERs and their uncertainties. Comparisons are made against the Ren et al. (2018) study which we abbreviate as R18. Only sites where ERs were calculated are included in the table. Some sites such as Rutledge NGCS did not yield increased emissions above background while others were intermittent (i.e., Cove Point LNG and Ellicott City NGCS).

Source Type	**Name**	**Dates Targeted**	**Max. Elevated CH_4 (ppb)**	**CH_4 ERs (g s^{-1})**	
				Our Study	R18
Landfills	Eastern Sanitary	03/03/25	64	267±204	213±250
	Harford Waste	07/23/25	74	71±26	141±78
	Reichs Ford	10/28/2025 (2x)	76	134±49	316±66
			112	204±70	
	Millersville	12/03/25	59	219±78	n/a
	Route 40 West	01/08/26	948	2232±1542	101±119
		**06/03/26	**430	**1340±1845	
	Brown Station	01/20/26 (2x)	755	1775±1422	497±106
			699	1282±1253	
Natural Gas Compressor Stations	Transco 190 (Ellicott City)	07/14/25	144	269±113	n/a
		07/23/25	328	248±115	
		12/03/25	131	110±34	
		01/08/26	224	308±230	
Liquified Natural Gas Facility	Cove Point	01/20/26	205	520±255	n/a

*ERs range from 66–2167 g s^{-1}.

**Results from Lawnmower+Sawtooth Configuration Flight (Section 5.3)

close to the surface precludes error analyses below the lowest flight altitude – a major limitation that we hope to resolve with future ground-mobile deployments.

Another target of interest was the Ellicott City NGCS. The first flight conducted over the Ellicott City NGCS resulted in an ER of 269±113 g s^{-1} on 14 July 2025. A follow-up flight nine days later on 23 July 2025 yielded a nearly identical ER of 248±115 g s^{-1}. The consistent signal from the Ellicott City NGCS and a lack of emissions from other NGCS's led to further investigations of the Ellicott City NGCS during the winter on 3 December 2025 and 8 January 2026. The first of the two winter flights resulted in the smallest ER calculated to date from the Ellicott City NGCS of 110±34 g s^{-1}, while a follow-up winter flight on 8 January 2026 yielded an ER of 308±230 g s^{-1} that was comparable to summer ER estimates. A decrease in the ER on 3 December 2025 compared to other days could be explained by differences in meteorological conditions. 3 December 2025, for instance, featured a northwesterly wind while all other instances either featured southwesterlies or westerlies. Northwesterlies are often associated with

https://doi.org/10.5194/egusphere-2026-6646
Preprint. Discussion started: 30 October 2026
© Author(s) 2026. CC BY 4.0 License.

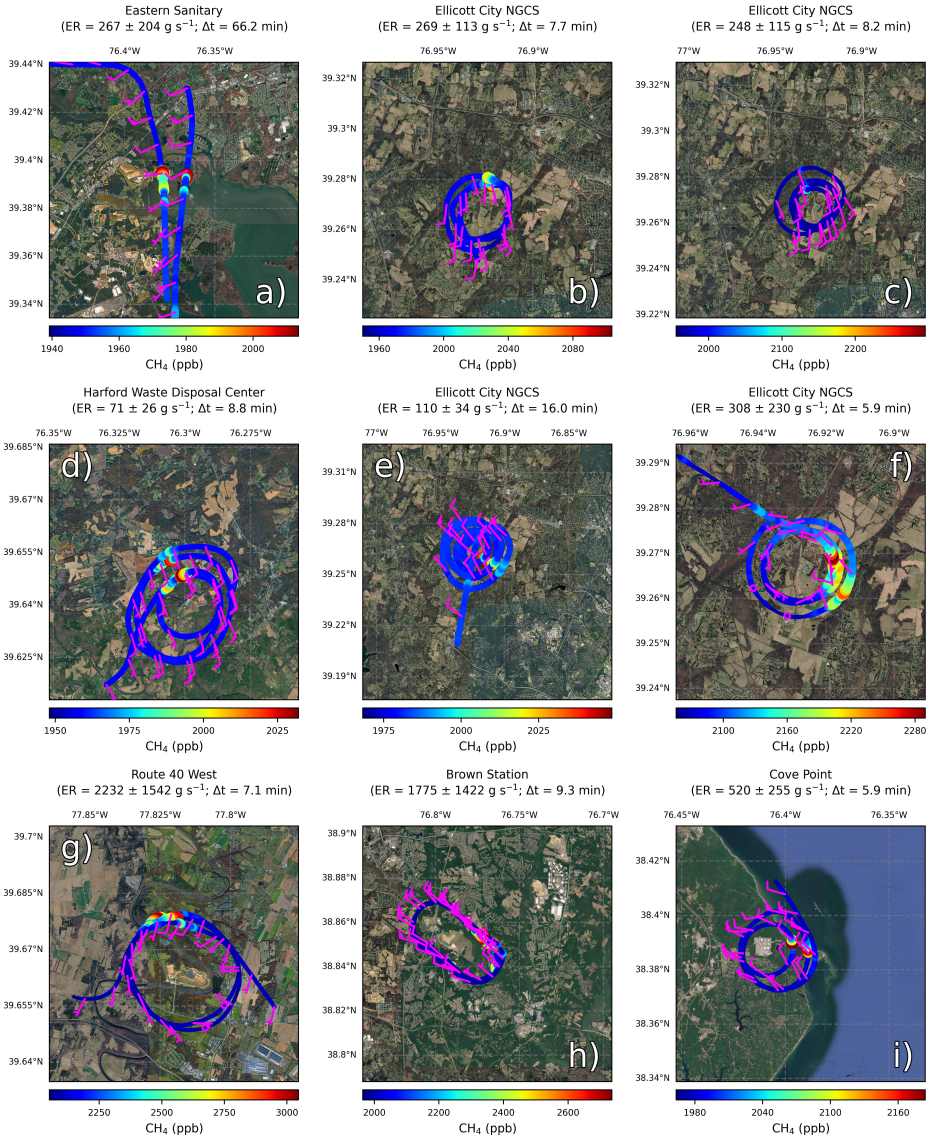

Figure 7. Flight paths conducted over targets of interest overlaid with CH_4 concentrations and flight-level winds measured near the a) Eastern Sanitary landfill on 3 March 2025, b) Ellicott City NGCS on 14 July 2025, c) Ellicott City NGCS on 23 July 2025, d) Harford Waste Disposal Center on 23 July 2025, e-f) Ellicott City NGCS on 3 December 2025 and 8 January 2026, g) Route 40 West landfill on 8 January 2026, h) Brown Station landfill on 20 January 2026, and i) Cove Point LNG facility on 20 January 2026. Included are ERs+uncertainties and the duration of loops conducted around GHG targets. ERs and uncertainties are also listed in Table 2. Google Earth imagery © 2025 Google.

https://doi.org/10.5194/egusphere-2026-6646
Preprint. Discussion started: 30 October 2026
© Author(s) 2026. CC BY 4.0 License.

high pressure moving into the region which increases the pressure tendency. Increased pressure tendencies can result in a suppression effect that reduces how much mass is emitted into the atmosphere (Xu et al., 2014). Interestingly, the ERs remained relatively consistent days and months after the initial survey. This suggests that frequent flights leveraging the CAP would be informative when addressing how much is emitted during a scheduled release or when identifying/mitigating leaks in compressor and piping infrastructure.

The last site targeted in Table 2 and shown in Figure 7i was an LNG facility at Cove Point. Surveys of this site are of interest because of the large quantity of CO_2 produced when natural gas is burned to power refrigeration compressors, and because of the potential release of unburned CH_4 during the cooling process in addition to venting and fugitive emissions (Balcombe et al., 2022; Innocenti et al., 2023). The CH_4 ER calculated from surveying Cove Point on 20 January 2026 was 520±255 g s^{-1}. We had flown to Cove Point two other days, with the first flight on 2 July 2025 and the second flight on 28 October 2025. The first flight also yielded significant CH_4 concentrations; however, the flight strategy did not support an ER calculation since measurements were conducted at only one altitude. The second flight did not yield any detectable emissions that day with concentrations resembling background CH_4. The highly variable emissions at the Cove Point LNG facility warrants further investigation. In the next section, we examine the LNG facility in a little more detail.

5.2 CO_2 and CH_4 Emissions from the LNG Facility at Cove Point

The flight to Cove Point on 20 January 2026 resulted in the interception of a GHG plume downwind of the LNG facility at three heights ranging from 350 m to 580 m as shown in Figures 7i and 8. The plumes were about 1.5 km to 2 km in width and decreased in concentration with height. Unlike the other sources analyzed, the LNG facility

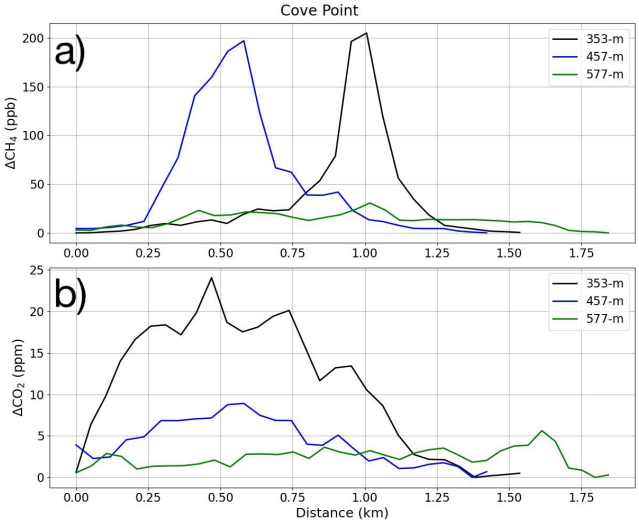

Figure 8. Isolated plumes from the Cove Point LNG facility during 20 January 2026 featuring a) CH_4 and b) CO_2 enhancements above background for three heights.

https://doi.org/10.5194/egusphere-2026-6646
Preprint. Discussion started: 30 October 2026
© Author(s) 2026. CC BY 4.0 License.

produced large amounts of CO_2 in addition to CH_4. At the lowest height flown, the maximum increase in CH_4 was 205 ppb while CO_2 reached 25 ppm above background. It is well known that LNG facilities produce far more CO_2 than CH_4 (e.g., Howarth, 2024; Zhang et al., 2023b). The ER for CO_2 determined at Cove Point was 220 ±127 kg s^{-1} or several hundred times greater than the CH_4 ER estimated. While the ER estimate seems high compared to the latest state GHG inventory (for year 2023), the roughly 870 tons hr^{-1} falls within the range of 100 to 1000 tons hr^{-1} that has been reported for LNG facilities (Zhang et al., 2023b). Furthermore, the results align with documented performance metrics for LNG production. The observed CH_4 leakage rate represents a minor loss of 0.007–0.045% per kilogram of LNG produced, which sits alongside a combustion and operational footprint of roughly 0.22 kg of CO_2 released for every kilogram of LNG produced. (Zhu et al., 2024). Future work will include more investigations of the LNG facility with a refined flight pattern featuring more loops around the source across a greater depth.

5.3 Volumetric Sampling of GHGs for Mass Balance: The Kriging Approach

The ERs calculated for the Brown Station and Route 40 West landfills in Section 5.1 were much larger than what Ren et al. (2018) reported. The application of Kriging to the lawnmower+sawtooth flight segments described in Section 4.3.2 was used as an alternative to capture the volumetric structure of the plume. Route 40 West was chosen as the pilot site for testing the Kriging approach and constructing the landfill plume onto a crosswind-height grid. Figure 9 shows over a dozen flight segments of the 3 June 2026 flight from near the source to 14.5 km downwind at ≈ 1 km spacing across heights ranging from 200 to 550 m. Concentrations were largest near the source and gradually decreased with downwind distance. The wind direction was nearly uniform and from the north during the flight, while wind speed exhibited moderate variability across the horizontal extent of the plume.

Combining gridded winds, temperature, and enhanced CH_4 (i.e., Figure 6d) as input into Equation (5) resulted in an ER of 1340±1845 g s^{-1} (42.29±58.23 kt CH_4/yr). Both the maximum concentration and average ER were about half of what was reported when conducting spirals around Route 40 West on 8 January 2026. It is difficult to say how much impact resulted from the method, differences in meteorological conditions and landfill operations, or seasonal variability of emissions. The uncertainties calculated follow the approach outlined in Section 4.3.2. Table 3 reports the breakdown of uncertainties and their relative errors. Varying the background by $3\sigma \pm 0.5\sigma$ and accounting for the standard deviation of wind direction about a circular mean (±13 degrees) resulted in the smallest relative uncertainties overall (i.e., 1.4 - 2.4%) owing to a nearly uniform wind direction and high confidence in background separation. Wind speed and varying R in Equation (6) by 0.25 and 4 led to moderate relative uncertainties of 32.9% and 47.1%, respectively. The largest relative uncertainty contribution was related to how the surface concentrations were represented prior to Kriging the data. Varying surface concentrations derived from the lowest altitude flight leg by 0.5 and 1.5x led to a relative uncertainty of 125.1%, which overwhelmingly dominated the root-sum of squares (RSS) calculation. The large uncertainty is the result of attempting to Krige derived surface concentrations multiplied by 0.5 and 1.5x across a 200 m gap extending from the surface to the lowest altitude flight segment. Coordination

https://doi.org/10.5194/egusphere-2026-6646
Preprint. Discussion started: 30 October 2026
© Author(s) 2026. CC BY 4.0 License.

with NOAA's ARC and drones to fill measurement gaps from the surface to the lowest altitude flight leg is planned in future work to constrain the lower portion of the plume.

Table 3. Uncertainty budget for the Kriging mass-balance emission rate.

Source	δF (kt/yr)	Relative (%)
Wind speed ($\pm 1.4\,\mathrm{m\ s^{-1}}$)	13.914	32.9
Wind direction ($\pm 13°$)	1.026	2.4
Kriging parameters (range × 0.25/4)	19.908	47.1
Background area ($\pm 0.5\sigma_G$)	0.609	1.4
Surface concentration ($\pm 50\%$)	52.907	125.1
Total (RSS)	**58.228**	**137.7**

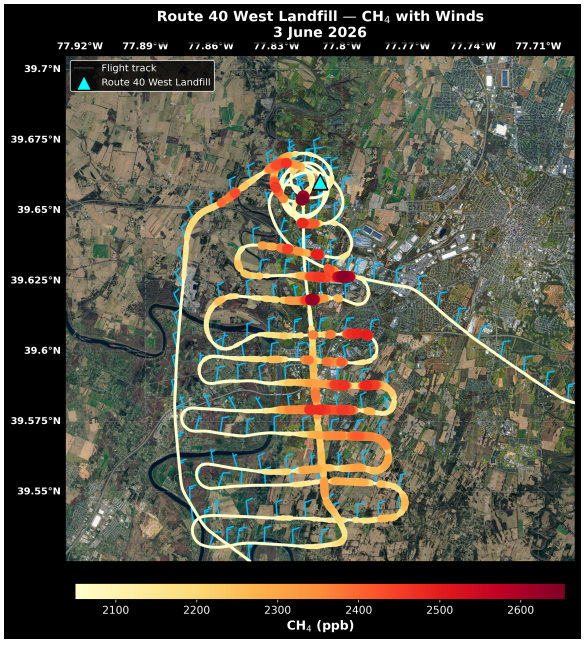

Figure 9. Volumetric survey of the Route 40 West landfill (cyan triangle) on 3 June 2026. The CAP flight track shaded by CH_4 concentration with flight-level winds overlaid as cyan barbs, showing the lawnmower pattern flown in the horizontal. Google Earth imagery © 2026 Google.

5.4 Coordinated Measurements Between CAP and NOAA's ARC

Measurements of emissions associated with a planned release at the Accident NGCS on 11 April 2026 were coordi-
570 nated with the CAP aircraft and NOAA's ARC based on information provided by the facility operator. Natural gas

https://doi.org/10.5194/egusphere-2026-6646
Preprint. Discussion started: 30 October 2026
© Author(s) 2026. CC BY 4.0 License.

was released from the pressurized pipeline in a "blowdown" event at a gradually declining rate over the course of 8 hours. NOAA's ARC operated and intercepted the plume at ground level repeatedly during much of the release, while the CAP aircraft intercepted the plume at flight level on four occasions during a 30 minute period about halfway through the event. Interceptions of the Accident NGCS plume were conducted at a single flight-level due to the presence of low clouds. ER calculations using the MBA were not considered in this analysis as a result of limited height sampling.

Figure 10a shows CH_4 measurements near and downwind of the Accident NGCS from NOAA's ARC and the CAP aircraft. Different colorbars were adopted in Figure 10a since concentrations from NOAA's ARC at the surface dwarfed flight-level concentrations. Plumes from the aircraft were isolated following Section 4.2. The peaks from NOAA'ARC were numerous, sharp, and dominated over the background signal. We used a baseline threshold that was about 100 ppb larger than background values derived from aircraft measurements to isolate plumes and conservatively select sharp peaks. Figure S4 shows NOAA's ARC and CAP aircraft plume measurements with a zoom-in of the section where plumes at flight level were isolated. Separating the plume segments from NOAA's ARC and comparing CH_4 and C_2H_6 in Figure 10b reveals a strong linear relationship with a correlation coefficient of 0.843 and slope indicating that C_2H_6 was 3.3% of CH_4. The 3.3% C_2H_6:CH_4 enhancement ratio is characteristic of dry thermogenic natural gas emissions typically associated with NGCS (Defratyka et al., 2021). Using the slope derived from Figure 10b, the average C_2H_6 concentration estimated for the plumes sampled by aircraft ranged from 20 to 50 ppb; a mention of the their uncertainties can be found in the figure caption. Future deployments of coordinated ground-based mobile and airborne measurements will take advantage of slope relationships to infer C_2H_6 ERs through the MBA.

6 Conclusions

A recent partnership between UMCP and CAP has led to a low-cost approach for conducting aerial surveys of GHGs and other environmental measurements in the state of Maryland. The availability of multiple aircraft, pilots, and instrument operators promotes a flexible weekly-to-biweekly flight schedule. The increase in the number of flights is ideal for addressing fugitive emissions, monitoring progress in curbing GHGs, and diagnosing causes of poor AQ.

In this paper, we discussed the implementation plan for successful CAP flights that included developing flight strategies for GHG surveys, site identification, instrument calibration, and post-processing of the data. Over two dozen flights have been conducted with the CAP since 2025 using a lightweight payload that consisted of a LI-7810 gas analyzer to measure CO_2, CH_4, and H_2O concentrations and a basic meteorological package. Coordination with MDE led to GHG emission targeting of key sites that included landfills, natural gas compressor stations, and a liquified natural gas (LNG) facility. The high frequency of flights conducted so far has supported surveys of specific targets across multiple days, and, in some instances, multiple times per day.

https://doi.org/10.5194/egusphere-2026-6646
Preprint. Discussion started: 30 October 2026
© Author(s) 2026. CC BY 4.0 License.

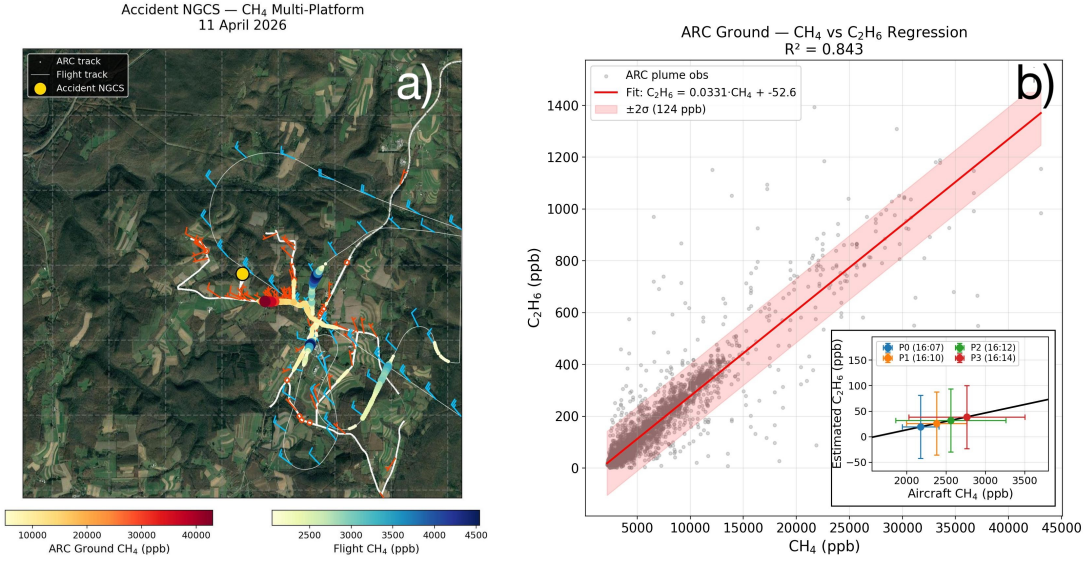

Figure 10. a) Coordinated CH_4 measurements between NOAA's Air Resources Car (ARC) and the CAP aircraft near the Accident NGCS (yellow circle) on 11 April 2026. The ARC ground track is shaded using the warm colorbar (left) with ARC-measured winds shown as red barbs, while the CAP flight track is shaded using the cool colorbar (right) with flight-level winds shown as blue barbs. Note that the two colorbars span very different ranges. Google Earth imagery © 2026 Google. b) C_2H_6 against CH_4 measured by NOAA's ARC within plumes sampled on 11 April 2026. Gray circles are individual ARC observations, the red line is the least-squares fit with the slope and offset reported in the legend, and the shaded band represents $\pm 2\sigma$ (124 ppb). An inset in b) shows the average CH_4 across each of the four plumes in their standard deviations (x-errorbar) and derived C_2H_6 with 2σ from a) representing y-errorbars.

The interception and isolation of plumes at different heights downwind of GHG sources allowed estimates of ERs under varying meteorological conditions and during different seasons. Frequent visits to targets as demonstrated in this study provide key insights into the variability of emissions that will be useful in improving the representativeness of bottom-up inventories important for modeling that cannot be accomplished by field deployments separated by multiple years (e.g., Schafer et al., 2025). Furthermore, frequent flights with CAP has supported adjustments to flight surveys of GHG plumes in order to examine the sensitivity to sampling strategies and their impact on ER calculations. Collaborations between facility operators was also demonstrated in coordination with CAP aircraft and NOAA's ARC during a planned release that enabled comparisons between platforms.

A flexible flight schedule, coordination with the MDE, and coordination with other measurement platforms demonstrates the CAP's effectiveness in frequent emissions targeting and in supporting broader environmental monitoring objectives. As the partnership with the CAP matures, a semi-permanent bi-weekly flight schedule will be implemented to continue monitoring GHG emissions and to determine sources of pollution that lead to poor AQ.

https://doi.org/10.5194/egusphere-2026-6646
Preprint. Discussion started: 30 October 2026
© Author(s) 2026. CC BY 4.0 License.

6.1 Future Direction

Several avenues are possible with the CAP that include coordination with facility operators and satellite validation. For instance, frequent flights conducted over the Ellicott City NGCS has piqued the interest of facility operators with conversations ongoing with UMCP about collaborating to address possible leaks contributing to CH_4 emissions. Discussions are also underway to implement research plans with landfill operators at Brown Station and Millersville. Coordination with GHGSat to validate ERs over targets of interest is also in the planning stages. Furthermore, additional coordinated measurements between NOAA's ARC and CAP are planned for targets of interest (e.g., the Ellicott City NGCS and the Brown Station landfill) and to derive C_2H_6 emission rates at flight level.

Each state has a dedicated CAP wing which means that substantial expansion is possible. Potential benefits of scaling this concept to other states include the validation of satellite retrievals across a myriad of locations subjected to different meteorological and surface conditions, the evaluation of bottom-up inventories, analyses of interstate transport, support measurements for climate studies and larger field deployments, and frequent monitoring of progress in curbing anthropogenic impacts.

Data availability. The data used in this study is published on Zenodo (Strobach, 2026).

Author contributions. ES, EJ, AT, RD, DL, JF, PS, and XR participated in preflight planning, flight strategies, and post-flight processing. XR, PS, and ES determined pressure dependence of the LI-7810 using a pressure chamber at NOAA ARL. JW provided guidance on GHG targets surveyed during flights. JD provided guidance on the meteorological outlook before scheduled flights. The CoURAGE led by KD supported detailed analyses of winds when determining transport conditions. XR led the deployment of NOAA's ARC and wrote the ARC section. ES, EJ, and DL conducted analyses of the data. ES wrote the manuscript and developed concepts therein. XR assisted in appropriately defining background concentrations and wind estimates near GHG targets for the mass balance approach. XR, JD, PW, JW, MR, RD, KD, and DL all reviewed the paper and made the necessary edits.

Competing interests. At least one of the (co-)authors is a member of the editorial board of Atmospheric Measurement Techniques.

Acknowledgements. The authors would like to acknowledge volunteers of the Maryland CAP wing for making flight-borne measurements possible. Claude.ai was used to enhance the visual representation of several figures.

https://doi.org/10.5194/egusphere-2026-6646
Preprint. Discussion started: 30 October 2026
© Author(s) 2026. CC BY 4.0 License.

References

Acker, S., Holloway, T., and Harkey, M.: Satellite detection of NO2 distributions using TROPOMI and TEMPO and comparison with ground-based concentration measurements, Atmospheric Chemistry and Physics, 25, 8271–8288, https://doi.org/10.5194/acp-25-8271-2025, 2025.

Ahn, D. Y., Hansford, J. R., Howe, S. T., Ren, X. R., Salawitch, R. J., Zeng, N., Cohen, M. D., Stunder, B., Salmon, O. E., Shepson, P. B., Gurney, K. R., Oda, T., Lopez-Coto, I., Whetstone, J., and Dickerson, R. R.: Fluxes of Atmospheric Greenhouse-Gases in Maryland (FLAGG-MD): Emissions of Carbon Dioxide in the Baltimore, MD-Washington, D.C. Area, Journal of Geophysical Research: Atmospheres, 125, e2019JD032 004, https://doi.org/10.1029/2019JD032004, 2020.

Balcombe, P., Heggo, D. A., and Harrison, M.: Total methane and CO2 emissions from liquefied natural gas carrier ships: the first primary measurements, Environmental science & technology, 56, 9632–9640, https://doi.org/10.1021/acs.est.2c01383, 2022.

Browning, K. and Wexler, R.: The determination of kinematic properties of a wind field using Doppler radar, Journal of Applied meteorology and climatology, 7, 105–113, https://doi.org/10.1175/1520-0450(1968)007<0105:TDOKPO>2.0.CO;2, 1968.

Bush, S., Hopkins, F., Randerson, J., Lai, C.-T., and Ehleringer, J.: Design and application of a mobile ground-based observatory for continuous measurements of atmospheric trace gas and criteria pollutant species, Atmospheric Measurement Techniques, 8, 3481–3492, https://doi.org/10.5194/amt-8-3481-2015, 2015.

Caicedo, V., Delgado, R., Luke, W. T., Ren, X., Kelley, P., Stratton, P. R., Dickerson, R. R., Berkoff, T. A., and Gronoff, G.: Observations of bay-breeze and ozone events over a marine site during the OWLETS-2 campaign, Atmospheric Environment, 263, 118 669, https://doi.org/10.1016/j.atmosenv.2021.118669, 2021.

Cambaliza, M., Shepson, P., Caulton, D., Stirm, B., Samarov, D., Gurney, K., Turnbull, J., Davis, K., Possolo, A., Karion, A., et al.: Assessment of uncertainties of an aircraft-based mass balance approach for quantifying urban greenhouse gas emissions, Atmospheric Chemistry and Physics, 14, 9029–9050, https://doi.org/10.5194/acp-14-9029-2014, 2014.

Cambaliza, M. O. L., Bogner, J. E., Green, R. B., Shepson, P. B., Harvey, T. A., Spokas, K. A., Stirm, B. H., and Corcoran, M.: Field measurements and modeling to resolve m2 to km2 CH4 emissions for a complex urban source: An Indiana landfill study, Elem Sci Anth, 5, 36, https://doi.org/10.1525/elementa.145, 2017.

Campbell, P. C., Tang, Y., Lee, P., Baker, B., Tong, D., Saylor, R., Stein, A., Huang, J., Huang, H.-C., Strobach, E., et al.: Development and evaluation of an advanced national air quality forecasting capability using the NOAA global forecast system version 16, Geoscientific model development, 15, 3281–3313, https://doi.org/10.5194/gmd-15-3281-2022, 2022.

Conley, S., Faloona, I., Mehrotra, S., Suard, M., Lenschow, D. H., Sweeney, C., Herndon, S., Schwietzke, S., Pétron, G., Pifer, J., et al.: Application of Gauss's theorem to quantify localized surface emissions from airborne measurements of wind and trace gases, Atmospheric Measurement Techniques, 10, 3345–3358, https://doi.org/10.5194/amt-10-3345-2017, 2017.

Cusworth, D. H., Jacob, D. J., Varon, D. J., Chan Miller, C., Liu, X., Chance, K., Thorpe, A. K., Duren, R. M., Miller, C. E., Thompson, D. R., et al.: Potential of next-generation imaging spectrometers to detect and quantify methane point sources from space, Atmospheric Measurement Techniques, 12, 5655–5668, https://doi.org/10.5194/amt-12-5655-2019, 2019.

Cusworth, D. H., Duren, R. M., Ayasse, A. K., Jiorle, R., Howell, K., Aubrey, A., Green, R. O., Eastwood, M. L., Chapman, J. W., Thorpe, A. K., Heckler, J., Asner, G. P., Smith, M. L., Thoma, E., Krause, M. J., Heins, D., and Thorneloe, S.: Quan-

https://doi.org/10.5194/egusphere-2026-6646
Preprint. Discussion started: 30 October 2026
© Author(s) 2026. CC BY 4.0 License.

tifying methane emissions from United States landfills, Science, 383, 1499–1504, https://doi.org/10.1126/science.adi7735, 2024.

Daley, H. M., Dickerson, R. R., Stratton, P. R., He, H., Ren, X., Koss, A., Brewer, A., Baidar, S., Hmiel, B., Bon, D., et al.: Methane and Ethane Emission Rates, Intensities, and Trends: Aircraft Mass Balance Insights over the Denver-Julesburg Basin, Fall 2021, Journal of Geophysical Research: Atmospheres, https://doi.org/10.1029/2025JD044370, 2026.

Davis, K., Zaitchik, B., Asa-Awuku, A., Bou-Zeid, E., Baidar, S., Boxe, C., Brewer, W. A., Chiao, S., Damoah, R., DeCarlo, P., et al.: Coastal-Urban-Rural Atmospheric Gradient Experiment (CoURAGE) Science Plan, Tech. rep., Oak Ridge National Laboratory (ORNL), Oak Ridge, TN (United States . . . , https://doi.org/10.2172/2429693, 2024.

Davis, K. J., Deng, A., Lauvaux, T., Miles, N. L., Richardson, S. J., Sarmiento, D. P., Gurney, K. R., Hardesty, R. M., Bonin, T. A., Brewer, W. A., et al.: The Indianapolis Flux Experiment (INFLUX): A test-bed for developing urban greenhouse gas emission measurements, Elem Sci Anth, 5, 21, https://doi.org/10.1525/elementa.188, 2017.

Defratyka, S. M., Paris, J.-D., Yver-Kwok, C., Loeb, D., France, J., Helmore, J., Yarrow, N., Gros, V., and Bousquet, P.: Ethane measurement by Picarro CRDS G2201-i in laboratory and field conditions: potential and limitations, Atmospheric Measurement Techniques, 14, 5049–5069, https://doi.org/10.5194/amt-14-5049-2021, 2021.

Dickerson, R. R., Stratton, P., Ren, X., Kelley, P., Heaney, C. D., Deanes, L., Aubourg, M., Spicer, K., Dreessen, J., Auvil, R., et al.: Mobile laboratory measurements of air pollutants in Baltimore, MD elucidate issues of environmental justice, Journal of the Air & Waste Management Association, 74, 753–770, https://doi.org/10.1080/10962247.2024.2393178, 2024.

Dreessen, J., Sullivan, J., and Delgado, R.: Observations and impacts of transported Canadian wildfire smoke on ozone and aerosol air quality in the Maryland region on June 9–12, 2015, Journal of the Air & Waste Management Association, 66, 842–862, https://doi.org/10.1080/10962247.2016.1161674, 2016.

Duren, R. M., Thorpe, A. K., Foster, K. T., Rafiq, T., Hopkins, F. M., Yadav, V., Bue, B. D., Thompson, D. R., Conley, S., Colombi, N. K., et al.: California's methane super-emitters, Nature, 575, 180–184, https://doi.org/10.1038/s41586-019-1720-3, 2019.

Dye, T., Chan, A., Anderson, C. B., Strohm, D., Wayland, R., and White, J.: From raw air quality data to the nightly news: an overview of how EPA's AIRNow program operates, in: Sixth Conference on Atmospheric Chemistry. American Meteorological Society annual meeting, Seattle, Washington, United States, pp. 12–16, https://ams.confex.com/ams/84Annual/techprogram/paper_72477.htm, 2004.

Fung, P. L., Al-Jaghbeer, O., Pirjola, L., Aaltonen, H., and Järvi, L.: Exploring the discrepancy between top-down and bottom-up approaches of fine spatio-temporal vehicular CO2 emission in an urban road network, Science of the Total Environment, 901, 165 827, https://doi.org/10.1016/j.scitotenv.2023.165827, 2023.

Gillespie, L. D., Ars, S., Worthy, C., Brantley, H., Green, R., Scarpelli, T. R., Cusworth, D. H., Vogel, F., and Wunch, D.: Comparison of Landfill Methane Emission Quantification Using Multiple Observation Methods, ACS Es&t Air, 2, 2786–2798, https://doi.org/10.1021/acsestair.5c00127, 2025.

Goldberg, D. L., Vinciguerra, T. P., Anderson, D. C., Hembeck, L., Canty, T. P., Ehrman, S. H., Martins, D. K., Stauffer, R. M., Thompson, A. M., Salawitch, R. J., et al.: CAMx ozone source attribution in the eastern United States using guidance from observations during DISCOVER-AQ Maryland, Geophysical research letters, 43, 2249–2258, https://doi.org/10.1002/2015GL067332, 2016.

https://doi.org/10.5194/egusphere-2026-6646
Preprint. Discussion started: 30 October 2026
© Author(s) 2026. CC BY 4.0 License.

Gordon, M., Li, S.-M., Staebler, R., Darlington, A., Hayden, K., O'Brien, J., and Wolde, M.: Determining air pollutant emission rates based on mass balance using airborne measurement data over the Alberta oil sands operations, Atmospheric Measurement Techniques, 8, 3745–3765, https://doi.org/10.5194/amt-8-3745-2015, 2015.

Guanter, L., Irakulis-Loitxate, I., Gorroño, J., Sánchez-García, E., Cusworth, D. H., Varon, D. J., Cogliati, S., and Colombo, R.: Mapping methane point emissions with the PRISMA spaceborne imaging spectrometer, Remote Sensing of Environment, 265, 112 671, https://doi.org/10.1016/j.rse.2021.112671, 2021.

He, H., Loughner, C. P., Stehr, J. W., Arkinson, H. L., Brent, L. C., Follette-Cook, M. B., Tzortziou, M. A., Pickering, K. E., Thompson, A. M., Martins, D. K., Diskin, G. S., Anderson, B. E., Crawford, J. H., Weinheimer, A. J., Lee, P., Hains, J. C., and Dickerson, R. R.: An elevated reservoir of air pollutants over the Mid-Atlantic States during the 2011 DISCOVER-AQ campaign: Airborne measurements and numerical simulations, Atmospheric Environment, 85, 18–30, https://doi.org/10.1016/j.atmosenv.2013.11.039, 2014.

Holben, B. N., Eck, T. F., Slutsker, I. a., Tanre, D., Buis, J., Setzer, A., Vermote, E., Reagan, J. A., Kaufman, Y., Nakajima, T., et al.: AERONET—A federated instrument network and data archive for aerosol characterization, Remote sensing of environment, 66, 1–16, https://doi.org/10.1016/S0034-4257(98)00031-5, 1998.

Howarth, R. W.: The greenhouse gas footprint of liquefied natural gas (LNG) exported from the United States, Energy Science & Engineering, 12, 4843–4859, https://doi.org/10.1002/ese3.1934, 2024.

Hu, H., Landgraf, J., Detmers, R., Borsdorff, T., Aan de Brugh, J., Aben, I., Butz, A., and Hasekamp, O.: Toward Global Mapping of Methane With TROPOMI: First Results and Intersatellite Comparison to GOSAT, Geophysical Research Letters, 45, 3682–3689, https://doi.org/10.1002/2018GL077259, 2018.

Huang, L., Stokes, S., Chen, Q., and Allen, D. T.: Uncertainties in the Estimated Methane Emissions in Oil and Gas Production Regions Based on Aircraft Mass Balance Flights, ACS Sustainable Chemistry & Engineering, 12, 11 024–11 032, https://doi.org/10.1021/acssuschemeng.4c03945, 2024.

Innocenti, F., Robinson, R., Gardiner, T., Howes, N., and Yarrow, N.: Comparative assessment of methane emissions from onshore LNG facilities measured using differential absorption lidar, Environmental Science & Technology, 57, 3301–3310, https://doi.org/10.1021/acs.est.2c05446, 2023.

Jacob, D. J., Varon, D. J., Cusworth, D. H., Dennison, P. E., Frankenberg, C., Gautam, R., Guanter, L., Kelley, J., McKeever, J., Ott, L. E., et al.: Quantifying methane emissions from the global scale down to point sources using satellite observations of atmospheric methane, Atmospheric Chemistry and Physics, 22, 9617–9645, https://doi.org/10.5194/acp-22-9617-2022, 2022.

Kang, M., Cho, S., Lee, Y., Lee, K.-H., Sohn, S., Choi, S.-W., Kim, J., and Park, J.: Quantification of methane and carbon dioxide surface emissions from a metropolitan landfill based on quasi-continuous eddy covariance measurement, Waste Management, 186, 355–365, https://doi.org/10.1016/j.wasman.2024.06.020, 2024.

Karion, A., Sweeney, C., Pétron, G., Frost, G., Michael Hardesty, R., Kofler, J., Miller, B. R., Newberger, T., Wolter, S., Banta, R., et al.: Methane emissions estimate from airborne measurements over a western United States natural gas field, Geophysical Research Letters, 40, 4393–4397, https://doi.org/10.1002/grl.50811, 2013.

Kljun, N., Calanca, P., Rotach, M., and Schmid, H. P.: A simple two-dimensional parameterisation for Flux Footprint Prediction (FFP), Geoscientific Model Development, 8, 3695–3713, https://doi.org/10.5194/gmd-8-3695-2015, 2015.

https://doi.org/10.5194/egusphere-2026-6646
Preprint. Discussion started: 30 October 2026
© Author(s) 2026. CC BY 4.0 License.

Kotsakis, A., Sullivan, J. T., Hanisco, T. F., Swap, R. J., Caicedo, V., Berkoff, T. A., Gronoff, G., Loughner, C. P., Ren, X., Luke, W. T., et al.: Sensitivity of total column NO2 at a marine site within the Chesapeake Bay during OWLETS-2, Atmospheric Environment, 277, 119 063, https://doi.org/10.1016/j.atmosenv.2022.119063, 2022.

Krautwurst, S., Gerilowski, K., Jonsson, H. H., Thompson, D. R., Kolyer, R. W., Iraci, L. T., Thorpe, A. K., Horstjann, M., Eastwood, M., Leifer, I., et al.: Methane emissions from a Californian landfill, determined from airborne remote sensing and in situ measurements, Atmospheric Measurement Techniques, 10, 3429–3452, https://doi.org/10.5194/amt-10-3429-2017, 2017.

Langford, A. O., Senff, C. J., Alvarez II, R. J., Aikin, K. C., Baidar, S., Bonin, T. A., Brewer, W. A., Brioude, J., Brown, S. S., Burley, J. D., et al.: The Fires, Asian, and Stratospheric Transport–Las Vegas Ozone Study (FAST-LVOS), Atmospheric Chemistry and Physics, 22, 1707–1737, https://doi.org/10.5194/acp-22-1707-2022, 2022.

Lauvaux, T., Miles, N. L., Deng, A., Richardson, S. J., Cambaliza, M. O., Davis, K. J., Gaudet, B., Gurney, K. R., Huang, J., O'Keefe, D., et al.: High-resolution atmospheric inversion of urban CO2 emissions during the dormant season of the Indianapolis Flux Experiment (INFLUX), Journal of Geophysical Research: Atmospheres, 121, 5213–5236, https://doi.org/10.1002/2015JD024473, 2016.

Loughner, C. P., Tzortziou, M., Follette-Cook, M., Pickering, K. E., Goldberg, D., Satam, C., Weinheimer, A., Crawford, J. H., Knapp, D. J., Montzka, D. D., et al.: Impact of bay-breeze circulations on surface air quality and boundary layer export, Journal of Applied Meteorology and Climatology, 53, 1697–1713, https://doi.org/10.1175/JAMC-D-13-0323.1, 2014.

McLinden, C., Griffin, D., Davis, Z., Hempel, C., Smith, J., Sioris, C., Nassar, R., Moeini, O., Legault-Ouellet, E., and Malo, A.: An independent evaluation of GHGSat methane emissions: Performance assessment, Journal of Geophysical Research: Atmospheres, 129, e2023JD039 906, https://doi.org/10.1029/2023JD039906, 2024.

Miller, M. A., Nitschke, K., Ackerman, T. P., Ferrell, W. R., Hickmon, N., and Ivey, M.: The ARM Mobile Facilities, Meteorological Monographs, 57, 9.1 – 9.15, https://doi.org/10.1175/AMSMONOGRAPHS-D-15-0051.1, 2016.

Ohyama, H., Yoshida, Y., and Matsunaga, T.: CH4 and CO emission estimates for megacities: deriving enhancement ratios of CO2, CH4, and CO from GOSAT-2 observations, Environmental Research Letters, 19, 124 025, https://doi.org/10.1088/1748-9326/ad89e0, 2024.

Peischl, J., Ryerson, T., Brioude, J., Aikin, K., Andrews, A., Atlas, E., Blake, D., Daube, B., De Gouw, J., Dlugokencky, E., et al.: Quantifying sources of methane using light alkanes in the Los Angeles basin, California, Journal of Geophysical Research: Atmospheres, 118, 4974–4990, https://doi.org/10.1002/jgrd.50413, 2013.

Pichugina, Y., Strobach, E., Brewer, A., Ahmadov, R., Bhattacharjee, P., James, E., Schnell, A., Carroll, B., Baidar, S., and Sandberg, S.: Analysis of Smoke Transport Over the Northeast US Caused by Wildfires in Canada During June 2023—Leveraging the HRRR-Smoke Model Predictions and Remote Sensing Observations, Journal of Geophysical Research: Atmospheres, 131, e2025JD044 799, https://doi.org/10.1029/2025JD044799, 2026.

Ren, X., Salmon, O. E., Hansford, J. R., Ahn, D., Hall, D., Benish, S. E., Stratton, P. R., He, H., Sahu, S., Grimes, C., Heimburger, A. M. F., Martin, C. R., Cohen, M. D., Stunder, B., Salawitch, R. J., Ehrman, S. H., Shepson, P. B., and Dickerson, R. R.: Methane Emissions From the Baltimore-Washington Area Based on Airborne Observations: Comparison to Emissions Inventories, Journal of Geophysical Research: Atmospheres, 123, 8869–8882, https://doi.org/10.1029/2018JD028851, 2018.

https://doi.org/10.5194/egusphere-2026-6646
Preprint. Discussion started: 30 October 2026
© Author(s) 2026. CC BY 4.0 License.

Roy, B., Mathur, R., Gilliland, A. B., and Howard, S. C.: A comparison of CMAQ-based aerosol properties with IMPROVE, MODIS, and AERONET data, Journal of Geophysical Research: Atmospheres, 112, D14 301, https://doi.org/10.1029/2006JD008085, 2007.

Ryerson, T., Andrews, A., Angevine, W., Bates, T., Brock, C., Cairns, B., Cohen, R., Cooper, O., De Gouw, J., Fehsenfeld, F., et al.: The 2010 California research at the Nexus of air quality and climate change (CalNex) field study, Journal of Geophysical Research: Atmospheres, 118, 5830–5866, https://doi.org/10.1002/jgrd.50331, 2013.

Schafer, N. B., Peischl, J., Apel, E. C., Barletta, B., Blake, D. R., Dass, P., DiGangi, J. P., Diskin, G. S., Francoeur, C., Fried, A., et al.: Trends in CH4 Emission Sources in the Los Angeles Basin from 2010 to 2023 Using Airborne Measurements, Environmental Science & Technology, https://doi.org/10.1021/acs.est.5c09817, 2025.

Stauffer, R. M., Thompson, A. M., Martins, D. K., Clark, R. D., Goldberg, D. L., Loughner, C. P., Delgado, R., Dickerson, R. R., Stehr, J. W., and Tzortziou, M. A.: Bay breeze influence on surface ozone at Edgewood, MD during July 2011, Journal of Atmospheric Chemistry, 72, 335–353, https://doi.org/10.1007/s10874-012-9241-6, 2015.

Strobach, E. J.: Data sets used in present study, https://doi.org/10.5281/zenodo.20491016, 2026.

Strobach, E. J., Baidar, S., Carroll, B. J., Brown, S. S., Zuraski, K., Coggon, M., Stockwell, C. E., Xu, L., Pichugina, Y. L., Brewer, W. A., et al.: An air quality and boundary layer dynamics analysis of the Los Angeles basin area during the Southwest Urban NO x and VOCs Experiment (SUNVEx), Atmospheric Chemistry and Physics, 24, 9277–9307, https://doi.org/10.5194/acp-24-9277-2024, 2024.

Strobach, E. J., Jaross, E., Ren, X., Dreessen, J., Walter, P., Wang, J. S., Park, J., Prince, N., Roots, M., Leblanc, T., Chouza, F., Dickerson, R. R., and Lathrop, D. P.: Synergistic Measurements of Air Quality in the Baltimore-Washington Region During a Bay Breeze: Exploiting CAP aircraft, TEMPO, Lidars, and Surface Networks, Atmospheric Chemistry and Physics (submitted), 2026.

Sullivan, J. T., Berkoff, T., Gronoff, G., Knepp, T., Pippin, M., Allen, D., Twigg, L., Swap, R., Tzortziou, M., Thompson, A. M., et al.: The ozone water–land environmental transition study: An innovative strategy for understanding Chesapeake Bay pollution events, Bulletin of the American Meteorological Society, 100, 291–306, https://doi.org/10.1175/BAMS-D-17-0025.1, 2019.

Tang, W., Worden, H. M., Deeter, M. N., Edwards, D. P., Emmons, L. K., Martínez-Alonso, S., Gaubert, B., Buchholz, R. R., Diskin, G. S., Dickerson, R. R., Ren, X., He, H., and Kondo, Y.: Assessing Measurements of Pollution in the Troposphere (MOPITT) carbon monoxide retrievals over urban versus non-urban regions, Atmospheric Measurement Techniques, 13, 1337–1356, https://doi.org/10.5194/amt-13-1337-2020, 2020.

Tao, L., Sun, K., Miller, D. J., Pan, D., Golston, L. M., and Zondlo, M. A.: Low-power, open-path mobile sensing platform for high-resolution measurements of greenhouse gases and air pollutants, Applied Physics B, 119, 153–164, https://doi.org/10.1007/s00340-015-6069-1, 2015.

Taubman, B., Hains, J., Thompson, A., Marufu, L., Doddridge, B., Stehr, J., Piety, C., and Dickerson, R.: Aircraft vertical profiles of trace gas and aerosol pollution over the mid-Atlantic United States: Statistics and meteorological cluster analysis, Journal of Geophysical Research: Atmospheres, 111, D10S07, https://doi.org/10.1029/2005JD006196, 2006.

Thorpe, A. K., Green, R. O., Thompson, D. R., Brodrick, P. G., Chapman, J. W., Elder, C. D., Irakulis-Loitxate, I., Cusworth, D. H., Ayasse, A. K., Duren, R. M., Frankenberg, C., Guanter, L., Worden, J. R., Dennison, P. E., Roberts, D. A., Chadwick,

https://doi.org/10.5194/egusphere-2026-6646
Preprint. Discussion started: 30 October 2026
© Author(s) 2026. CC BY 4.0 License.

K. D., Eastwood, M. L., Fahlen, J. E., and Miller, C. E.: Attribution of individual methane and carbon dioxide emission sources using EMIT observations from space, Science Advances, 9, eadh2391, https://doi.org/10.1126/sciadv.adh2391, 2023.

Turnbull, J. C., Karion, A., Davis, K. J., Lauvaux, T., Miles, N. L., Richardson, S. J., Sweeney, C., McKain, K., Lehman, S. J., Gurney, K. R., et al.: Synthesis of urban CO2 emission estimates from multiple methods from the Indianapolis Flux Project (INFLUX), Environmental science & technology, 53, 287–295, https://doi.org/10.1021/acs.est.8b05552, 2018.

Xu, L., Lin, X., Amen, J., Welding, K., and McDermitt, D.: Impact of changes in barometric pressure on landfill methane emission, Global Biogeochemical Cycles, 28, 679–695, https://doi.org/10.1002/2013GB004571, 2014.

Yahya, K., Zhang, Y., and Vukovich, J. M.: Real-time air quality forecasting over the southeastern United States using WRF/Chem-MADRID: Multiple-year assessment and sensitivity studies, Atmospheric Environment, 92, 318–338, https://doi.org/10.1016/j.atmosenv.2014.04.024, 2014.

Zhang, S., Ma, J., Zhang, X., and Guo, C.: Atmospheric remote sensing for anthropogenic methane emissions: Applications and research opportunities, Science of The Total Environment, 893, 164 701, https://doi.org/10.1016/j.scitotenv.2023.164701, 2023a.

Zhang, Z., Cusworth, D. H., Ayasse, A. K., Sherwin, E. D., and Brandt, A. R.: Measuring carbon dioxide emissions from liquefied natural gas (LNG) terminals with imaging spectroscopy, Geophysical Research Letters, 50, e2023GL105 755, https://doi.org/10.1029/2023GL105755, 2023b.

Zhao, X., Griffin, D., Fioletov, V., McLinden, C., Liu, X., Park, J., Petropavlovskikh, I., Hanisco, T. F., Szykman, J., Valin, L., Baumann, E., Cede, A., Tiefengraber, M., Gebetsberger, M., Uesato, I., Zheng, X., Ahn, S., Chang, L., Lee, W.-J., Kim, J. H., Lee, H., Baek, K., Redondas, A., Fujiwara, M., Wang, T., Grutter, M., Houck, J. C., Haffner, D., and Lee, S. C.: Geostationary Satellites Total Ozone Observations: First Results on Ground-Based Networks Validation Efforts for TEMPO and GEMS, Geophysical Research Letters, 52, e2025GL114 768, https://doi.org/10.1029/2025GL114768, 2025.

Zhu, Q., Davidson, E. A., Hagedorn, J. G., Castro, M. S., Fisher, T. R., Fox, R. J., Brown, S. E., and Lewis, J. W.: Quantification of soil N2O and CH4 fluxes using the flux gradient method on a drainage water managed farm on the eastern shore of Maryland, Agricultural and Forest Meteorology, 343, 109 762, https://doi.org/10.1016/j.agrformet.2023.109762, 2023.

Zhu, Y., Ross, G., Khaliukova, O., Roman-White, S. A., George, F. C., Hammerling, D., and Ravikumar, A. P.: Multiscale measurements of greenhouse gas emissions at US natural gas liquefaction terminals, Environmental Science & Technology Letters, 12, 44–50, https://doi.org/10.1021/acs.estlett.4c00713, 2024.